sustainability

Article

Evaluation of General Circulation Models CMIP6 Performance and Future Climate Change over the Omo River Basin, Ethiopia

Tolera Abdissa Feyissa [1,2,*], Tamene Adugna Demissie [2], Fokke Saathoff [1] and Alemayehu Gebissa [1]

[1] Geotechnics and Coastal Engineering, Faculty of Agricultural and Environmental Sciences, Rostock University, 18059 Rostock, Germany
[2] Faculty of Civil and Environmental Engineering, Jimma University, Jimma 378, Ethiopia
* Correspondence: tolera.feyissa@uni-rostock.de or toleraabdissa@yahoo.com; Tel.: +49-15123595056

Abstract: One of the world's major issues is climate change, which has a significant impact on ecosystems, human beings, agricultural productivity, water resources, and environmental management. The General Circulation Models (GCMs), specially the recently released (coupled model intercomparison project six) CMIP6 are very indispensable to understand and support decision makers to identify adaptation strategies in response to future climate change in a basin. However, proper selection of skillful GCMs and future climate assessment is a prior task to climate impact studies. The objective of the study is an attempt to appraise the climate model's performance and future climate scenarios of Shared Socioeconomic Pathways (SSPs) in the Omo River Basin. The performance evaluation of 20 GCMs of the CMIP6 was properly performed to reproduce the precipitation and the maximum temperature in the basin. Their performance has been carried out against the best selected mean monthly Climate Hazards Group InfraRed Precipitation with Station (CHIRPS) precipitation and European Community Medium Water Range Weather Forecasts Version 5 (ECMWF-ERA5) maximum temperature. The GCMs of the CMIP6 were selected and ranked using the compromise programming method of multi-criteria decision making. The result shows that ensemble models and NorESM2-MM models have been designated to reproduce the precipitation and maximum temperature in the basin respectively. The Mann–Kendall trend test was executed to appraise the trend of selected CMIP6 models, and subsequently, downscaling and bias correction techniques were conducted. The projected seasonal precipitation of June, July, August, September (JJAS) and March, April, May (MAM) shows an increasing trend with 10.86, 17.66, 38.96 and 11.85, 22.1, and 40.7% under SSP2452031-2060, SSP5852031-2060, and SSP5852071-2100 scenarios respectively. Furthermore, increasing trends were detected in MAM by 12.8% and decreasing trends in JJAS were detected by 15.23% under SSP2452071-2100 scenario. The maximum temperature projection will be increased on average by 0.95, 1.78, 1.4, and 3.88 °C in JJAS and 1.53, 2.24, 1.56, and 3.89 °C in MAM under climate change scenarios of near-future SSP2452031-2060, SSP5852031-2060, far-future SSP2452071-2100, and SSP5852071-2100, respectively. Additionally, the basin has shown temporal-spatial climate fluctuation in terms of precipitation and maximum temperature.

Keywords: climate projection; CMIP6 performance; compromise programming; Omo River Basin; precipitation; temperature

Citation: Feyissa, T.A.; Demissie, T.A.; Saathoff, F.; Gebissa, A. Evaluation of General Circulation Models CMIP6 Performance and Future Climate Change over the Omo River Basin, Ethiopia. *Sustainability* **2023**, *15*, 6507. https://doi.org/10.3390/su15086507

Academic Editor: Ozgur Kisi

Received: 16 February 2023
Revised: 30 March 2023
Accepted: 1 April 2023
Published: 12 April 2023

1. Introduction

Climate change is one of the most dangerous problems facing the world today, both in terms of its universal context and how it responds to environmental and socioeconomic forces [1]. The sixth assessment report (AR6) indicates that the scope and intensity of climate change consequences are greater than predicted by earlier assessments. Due to climate change, there has been widespread degradation of ecosystem resilience, natural adaptive capacity, as well as alterations in seasonal timing (IPCC, 2022) [2]. Because it has caused the climate system to undergo unprecedented change, it has increased weather severity and frequency (temperature and precipitation patterns [3], which will have an effect on the spatial -temporal hydrological cycle [4–6].

Africa is among the continents most affected by climate change and is particularly susceptible to its effects, such as drought and floods brought on by rising air temperatures and shifting precipitation patterns, which threaten agriculture, water security, and socioeconomic development [7–11]. For instance, Kenya and Ethiopia in East Africa have seen more than 3 million cattle deaths, because of water scarcities, considerable vegetation deficits [12], and lack of climate change adaptation potential [13,14]. Ethiopia's economy is heavily dependent on rainy season agriculture, which is extremely susceptible to the impact of climate change, particularly variations in precipitation trends [15].

The Omo River Basin is one of the main transboundary river basins of Ethiopia, and located in the southwest of the country. It has significant potential runoff close to the Abay and Baro Akobo river basins in the country and accounts for 22.7% of the hydroelectric power potential next to the Blue Nile River basin [16]. However, the basin is susceptible to climate change due to the substantial temporal variations in temperature and precipitation [17]. According to studies on how climate change would affect the basin's water resources [18–20], stream flows increase during the rainy season and fall in the dry because of significant variations in both temperature and precipitation that are predicted. However, the results of several studies that have been done in the basin show a decreasing stream flow in the basin under all seasons and climate projection scenarios [21]. These researchers utilized a limited number of GCMs to analyze how climate change would affect the basin, and the discrepancies between their findings and the higher rainfall variability in the basin could be caused by a lack of sufficient temporal-spatial data.

The investigation of climate change, and understanding its consequence is essential to informing the decision and policy makers when making adaptions and designing infrastructure to withstand future conditions [4]. GCMs are used to replicate the pattern of climate in order to have a better awareness about climate change with its implications on the past, present, and future ecosystems [22]. GCMs are vigorous in assessing climate change impact, and simulations shared across different CMIP phases are essential to provide measurable projections of climate for the 21st century [23,24]. The CMIP phase 3 (CMIP3) GCM simulations [25] had been used to prepare the IPCC fourth assessment report (AR4) [26]. The CMIP5 models improved upon the CMIP3 models with respect to physical processes and network precision [27]. The results of a comparison between the CMIP3 and CMIP5 models revealed that the CMIP5 performed better in reproducing the observed climate in numerous places and large-scale air circulations that affect the climate of a region [28,29].

The World Climate Research Programme (WCRP) has currently launched state-of-the-art climate model experiments known as the CMIP6 which represents the latest climate modeling data for these study types. These experiments are being conducted to produce historical, present, and future scenarios for the global community of climate modelers. The WCRP CMIP information can be found at https://www.wcrpclimate.org/wgcm-cmip and was accessed on 10 June 2022. The higher spatial resolutions, improved cloud microphysical process parameters, biogeochemical cycles, and additional Earth system processes are made different from the CMIP6 from previous versions [24,30]. In addition to the Representative Concentration Pathway (RCP) of CMIP5 and the Shared Socioeconomic Pathways (SSPs), the CMIP6 considers three new emission pathways that have been included to fill the gap between the typical pathways of CMIP5 [31,32]. These scenarios are used to analyze how societal actions will affect greenhouse gas (GHG) emissions and how the Paris Agreement's climate targets will be met. The shared SSPs can be applied to assess the climate models' capability at various time scales and to create the groundwork for the prediction of future climate because they are seen as more realistic future scenarios [33].

However, a significant problem in projections of climate change and impact analyses is an acceptable GCMs subset selection. All GCMs cannot be used to replicate accurate future climate projections at the basin and sub-basin levels due to the high levels of uncertainty associated with their simulations [34–36]. Some sources of these uncertainties are: the resolution of the model, mathematical formulation, initial assumptions, and processes of calibration. In order to reduce projection uncertainty, omitting GCMs subset models show that less skill at mimicking the observed climate is preferred [34,37]. The climate modeling community, according to [38,39], is mostly focused on the GCMs' temporal performance while ignoring the explicit evaluation of their spatial performance, which is also crucial. In fact, the spatial performance variations of GCMs exist on the ground [34,40]. To lessen the uncertainties related to the GCMs, some researchers have suggested that a multi-model ensemble (MME) be assembled from a GCM pool by removing the GCMs that indicate less ability of simulation [36,41,42]. Contrarily, the efficiency of uncertainty removal is a big challenge for the majority of GCMs, making the combining of many GCMs models for the projection of climate difficult [43].

Furthermore, there is the issue of identifying statistical metrics' performance that appropriately correspond to the model's predictive abilities, as well as the problem of a general model ranking approach that is versatile in the model's subset selection [44]. In the past, studies have been undertaken to assess the ability of GCMs globally using a variety of statistical indicators [45–48]. However, due to inconsistencies in the results of many statistical metrics, selecting which GCMs performed best can be difficult [49,50]. This puts the emphasis on using a compromise approach that can take into account trade-offs while choosing optimal models. To reduce this uncertainty, multi-criteria decision-making (MCDM) is a technique that integrates statistical and numerical results for computing weights/values of the criteria of statistical metrics [51–53], and ranking the GCMs [54,55]. In particular, Compromise Programming (CP) is one of the more effective MCDM strategies that has the ability to distinguish between the nearby ideal and best solution in comparison to other MCDM procedures [56,57]. In individually optimizing each criterion, the unreachable perfect solution can be found for every well-bound set of possibilities.

Climate model selection is performed in order to predict future precipitation and temperature for the study area. Selecting an appropriate GCM for a particular area is the most important task when evaluating the effects of climate change on various sectors [58]. The evaluation of CMIP6 model performance was successfully carried out for reproducing air temperature in the Arid Area of Northwest China and its subregions [59]. In Pakistan, CMIP6 multi models' evaluation and selection were conducted based on spatial assessment metrics for simulation of precipitation and maximum and minimum temperature [36]. In the same manner, evaluation and projection of CMIP6 over East Africa [60] and in Ethiopia, Upper Awash, and the Upper Blue Nile Basin were done by [61,62] respectively at basin level, which was not sufficient. Even though the Omo River Basin has tremendous resource potential for hydroelectric power, irrigation, and other uses, the GCM's performance evaluation and effect analysis are not given much attention. The performance evaluation of the CMIP6 GCMs and their future climate scenarios has not yet been done for the Omo River Basin. Therefore, this research was an attempt to evaluate the performance of GCMs of the CMIP6 and future climate trends under SSP scenarios for both the impact analysis of future climate change on hydrology and adaptation strategies in the basin.

2. Materials and Methods

The Omo River Basin is situated in the southwest of Ethiopia, between the Oromia Regional State and the Southern Nations, Nationalities, and Peoples' Region, between latitudes $4°00'$ and $9°22'$ and longitudes $34°44'$ and $38°24$ as shown in the Figure 1. The basin is 550 km long, with a surface area of 79,000 km^2, and an average width of 140 km (SDCSE, 2013). The Omo River flows through Ethiopia's torrid lowlands after rising in the Oromia region of the Shewa highlands. Gibe River and Gojeb River are the two principal rivers that drain it. The Walga and Wabe rivers are the two largest tributaries in the basin's northern region. According to South Design and Construction Supervision Company and Water Works Design Supervision Enterprise (SDCSE, 2013), the Tuljo and Gilgel Gibe rivers flow into the Gibe.

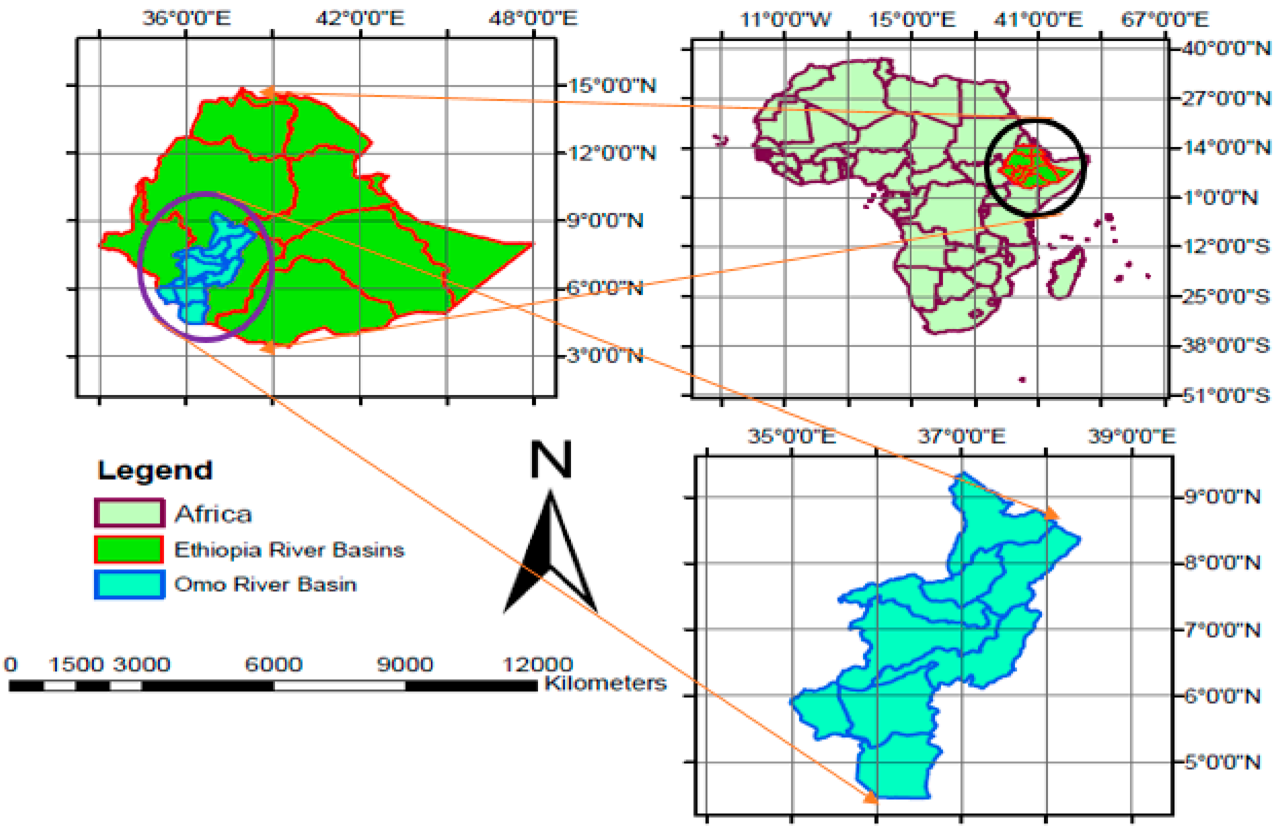

Figure 1. Map of the study area.

About 90% of Lake Turkana's annual input is provided by the river, which has an annual flow of 16.6 BMC. It has the second highest hydroelectric power generation potential in the country, next to the Blue Nile River basin, with 22.7%. From five cascade hydroelectric power plants in the basin, three of them are operating, one under construction and the left is not yet started. The basin has a 383,000-ha irrigation potential (FAO, 2017), with the lower basin part slated to be Ethiopia's greatest irrigated area for agricultural growth. A 41 km long canal is being built in the region by the Ethiopian Construction Works Company, and it will provide 125,000 m^3 of water for irrigation. Seven sugar plant companies that would use water from this water canal are planned for this area, together with a government-run plantation covering 200,000 hectares.

The basin's higher land part receives an average annual rainfall of 1900 mm and the southern lowland gets less than 400 mm per year. The basin has an average annual maximum temperature that varies from 23 °C to 17 °C in the northwestern highlands and more than 29 °C in the southern lowlands [63]. There is high topography variation in the basin [64]. In the northern part of the basin, two-thirds of the topography is hilly and cut by the deeply incised gorges of the rivers. One-third is a flat alluvial plain punctuated by hilly areas in the southern. The topography of the elevation varies from 1500–3360 m a.s.l. in the northern and central parts of the basin, and 400–500 m a.s.l in the southern lower part of the basin.

2.1. Observed Data Set

For the evaluation of climate model performance and impact analysis, a basin's meteorological data is absolutely essential [65]. The daily observed data was collected from the Ethiopian Meteorological Service Agency (EMSA) from 1985–2014. There were 20 stations of precipitation and 16 stations with maximum and minimum temperatures. However, certain stations' data contained missing data, and the INSTAT's Markov chain simulation model was used to estimate the missing data [66]. For many developing

African countries, including Ethiopia, the accuracy of climatic data poses a significant challenge [67]. This problem was solved by carefully assessing and analyzing the quality of the daily observed data. Accordingly, checking false zeros, the homogeneity test, and outliers were performed using Climate Data Tool (CDT). Climate Data Tool (CDT) is an open-source, R-based software with an easy-to-use graphical user (interface (GUI) and is available on the website of https://github.com/rijaf-iri/CDT [68].

2.2. Gauged Based Gridded Data

The high resolution of spatial-temporal observed data is very important to understanding the consequence of future climate variation at the basin and sub-basin level. However, regions in developing countries, such as Ethiopia, with limited ground observations, are extremely sensitive to climate hazards [69]. It is quite uncommon in Africa to obtain climatic data of high quality from meteorological field stations [70].The inconsistencies between various data products are mostly caused by a small number of ground stations, inadequate time resolution in merging and interpolation methods [71,72], and limited documentation quality. In contrast, gridded datasets are routinely used to select a subset of the available models and are crucial for evaluating current climate models. Griddled datasets are necessary in order to correct or adjust the regional scale biases that persist in climate models. In the present study, the Climate Hazards Group Infrared Precipitation with Stations (CHIRPS) environmental record is a new precipitation dataset developed by the US Geological Survey (USGS) and the Climate Hazards Group at the University of California, Santa Barbara (UCSB) [73], Climatic Research Unit (CRU version TS4.04) from the University of East Anglia [74], Climate Prediction Center (CPC) dataset established by the NOAA Climate Prediction Center, National Centers for Environmental Prediction [53,75], and the Global Precipitation Climatology Centre (GPCCv2022) [76]; reanalysis products are also derived from European Community Medium Water range Weather Forecasts v5 (ECMWF-ERA5) [77,78], and have been used to appraise the performance of GCM CMIP6 models.

2.3. GCMs Dataset

A total of 20 CMIP6 GCM simulations have been downloaded as revealed in the Table 1 and evaluated to reproduce the precipitation and temperature in this study area. These climate models' data were downloaded from the website of the Earth Systems Grid Federation (ESGF); https://esgf-node.llnl.gov/search/cmip6/) [24]. The historical data of GCMs CMIP6 from 1985–2014 and for future projection, the shared socio-economic pathways (SSPs) medium forcing scenario (SSP2-4.5, and a strong forcing scenario (SSP5-8.5) were used. The purpose of the SSPs was to provide a unified analysis of future climate vulnerabilities, impacts, adaptation, and mitigation. They were created by the community of researchers studying climate change [79]. The scenarios' detailed explanation is accessible in [80,81].

Table 1. Name of GCMs CMIP6 models used with their country, resolution, and references.

S.No.	GCMs CMIP6 Name	Country	Horizontal Res (lon. lat. deg)	Key References
1	ACCESS-CM2	Australia	$1.87° \times 1.25°$	[82]
2	ACCESS-ESM1-5	Australia	$1.9° \times 1.2°$	[83]
3	BCC-CSM2-MR	China	$1.1° \times 1.1°$	[84]
4	CanESM5	Canada	$2.8° \times 2.8°$	[85]
5	CMCC-ESM2	Italy	$0.94° \times 1.25°$	[86]
6	GFDL-CM4	USA	$2.50° \times 2.00°$	[87]
7	GFDL-ESM4	USA	$1.00° \times 1.25°$	[88]
8	INM-CM4-8	Russia	$2° \times 1.5°$	[89]
9	IPSL-CM6A-LR	France	$2.50° \times 1.27°$	[90]
10	INM-CM5-0	Russia	$2.00° \times 1.50°$	[89]

Table 1. *Cont.*

S.No.	GCMs CMIP6 Name	Country	Horizontal Res (lon. lat. deg)	Key References
11	KACE-1-0-G	South Korea	$1.9° \times 1.3°$	[91]
12	KIOST-ESM	Korea	$2.2° \times 2.2°$	[92]
13	MIROC6	Japan	$1.4° \times 1.4°$	[93]
14	MPI-ESM1-2-HR	Germany	$0.94° \times 0.94°$	[94]
15	MPI-ESM1-2-LR	Germany	$1.87° \times 1.86°$	[95]
16	MRI-ESM2-0	Japan	$1.1° \times 1.1°$	[96]
17	NESM3	China	$1.9° \times 1.9°$	[97]
18	NorESM2-LM	Norway	$2.5° \times 1.9°$	[98]
19	NorESM2-MM	Norway	$0.9° \times 1.3°$	[98]
20	TaiESM1	Taiwan	$0.9° \times 0.9°$	[99]

2.4. Selection of Performance Criteria and GCMs CMIP6 Models

Recently, gridded data has become the most important to examine the replication ability of the GCMs CMIP6 climate models in the basin. The replication ability of gauge-based gridded data for the observation are various. However, several studies have not statistically compared the gridded data with the observed data in the basin in order to assess the performance of climate models [44] in Nigeria, such as ref. [22] in North Africa and [100] in Ethiopia. In this study, to alleviate such a gap, we have evaluated the gridded data against the ground observation data statistically to select the best reference data. Accordingly, the mean monthly precipitation and temperature gridded data were appraised against the monthly observational data in the basin using statistical indicators such as the root mean square error (RMSE), coefficient of correlation (CC), mean bias (MB), and Nash–Sutcliffe Efficiency (NSE). Similarly, choosing the appropriate performance criteria or indicators is a prerequisite for ranking climate models based on the skill of their simulation. However, clearly approved performance indicators do not exist to evaluate and rank the climate models. The selection of the indicators was carried mainly based on category of the time-domain and frequency-domain based metrics [101,102].

Accordingly, the simulation skill of the 20 GCMs over the Omo River Basin (1985–2014) against the mean monthly reference data set were assessed using statistical measures metrics such as NSE [103,104], the percent of bias (PBIAS %), Normalized root mean square error (NRMSE) [105,106], the correlation coefficient (CC) [107], and skill score (SS) [108]. Furthermore, the degree to which the patterns agree with ground data was shown graphically via a Taylor diagram [109,110]. It uses a single diagram to compare the temporal performance of climate models to monthly observations and reanalysis, taking into account three indicators' metrics such as correlation coefficient, centered (unbiased) RMSE, and standard deviation. On the other hand, all these indicators' metrics have their own weaknesses and strengths, and there are a variation of climate model evaluation metrics [111]. To discuss these issues, MCDM methods were used to aggregate multiple performance indicators into a single measure. We have used the Compromise Programming of MCDM technique for selecting the model using indicator metrics, and its brief discussion is given as follow.

2.5. Evaluation of CMIP6 Models Performance Using MCDM Method

As compromise programming (CP) is a method that can be used to measure the cumulative impact of many statistical indices, it was used to evaluate and rank GCMs CMIP6 models [112]. Since any decision-maker prefers a solution that is as close to the ideal as possible, compromise programming is quite practical, and several scholars have applied it for the ranking of climate models [44,55,113–115]. Previously, the compromise programming MCDM technique for ranking global climate models has not been implemented before in the study area. Ranking GCMs CMIP6 models were done based on the LP value, which represents the smallest distance between the normalized values and the ideal values performance indicator metrics. Before this, the weight of each performance indicator metric was calculated by the entropy method [55,116]. The following are step-by-step expressions for the entropy approach (Equations (1)–(4));

$$K_{aj}=\frac{K_j(a)}{\sum_{a=1}^{T}K_j(a)} \tag{1}$$

$$En_j=-\frac{1}{\ln(T)}\sum_{a=1}^{T}K_{aj}\ln\left(K_{aj}\right) \tag{2}$$

$$D_{dj}=1-En_j \tag{3}$$

$$r_j=\frac{D_{dj}}{\sum_{j=1}^{J}D_{dj}} \tag{4}$$

Lastly, each normalized indicator's distance from its normalized ideal values (Lp) was calculated (Equation (5)) to determine the models' rank.

$$L_{pa}=\left[\sum_{j=1}^{J}r_j^p\left|K_J^*-K_j(a)\right|^p\right]^{\frac{1}{p}} \tag{5}$$

where K_{aj} denotes the normalized value of error indices, $K_j(a)$ is the value of the chosen indicator j for GCM a; T denotes the total number of GCMs, a is index for GCMs; (j = 1, 2, . . . , J) where J is maximum number of indicators, En_j denotes the entropy of every single indicator for j, D_{dj} denotes the degree of diversification, and r_j represents the normalized weight of indicators. L_{pa} = Lp metric for GCMs for the chosen value of parameter p; K_J^* = Normalized ideal value of indicator j; p = Parameter (1 for linear, 2 for squared Euclidean distance measure).

2.6. Trend Analysis of Future Climate Projection

The mean monthly future climate projections analysis was carried out for temperature, and precipitation over a 30-year time frame for the baseline period (1985–2014), near-future period (2031–2060) and far-future period (2071–2100). The hydro-meteorological data has been examined using a variety of statistical techniques, most of which fall under the categories of variability and trend analysis [117,118]. In the presented study, the Mann–Kendall (MK) trend test method was applied for future change analysis of the temperature and precipitation data using RStudio tool. A non-parametric technique called the Mann-Kendall (MK) test is used to identify trends in time series of climate data. The Mann-Kendall test has been commonly used in numerous trend studies; such as in refs. [11,14,119,120], for temporal trend analysis and is preferable to parametric analysis for climate variables trend assessments [121]. Non-parametric trend does not require normal distribution in datasets to handle outliers and missing values. A non-parametric test has limited sensitivity to short breaks due to the inhomogeneity of the time series [122]. The null hypothesis, which states that the data series is serially independent and uniformly distributed with no trend, and the alternative hypothesis, which states that a trend exists in the data series, serve as the foundation for the assumption. Furthermore, the magnitude of the MK test statistic provides a clear indication of the trend's strength, with higher magnitudes exhibiting more powerful trends and lower magnitudes indicating a weaker trend.

The value of the normalized test statistics (Z) was used to test whether the trend was increasing or decreasing. The trend is considered to be increasing when Z is positive and declining when Z is negative. In this study, the significance is determined based on the *p*-value at a significance threshold of 0.05. As a result, the data exhibits a significant trend if the *p*-value is less than or equal to 0.05, while the null hypothesis that the data do not exhibit significant trends is accepted if the *p*-value is greater than 0.05.

3. Results

3.1. Gauged Based Gridded Dataset

The monthly observed precipitation and temperature data of the Omo River Basin have been used to evaluate the gridded data for 30 years (1985–2014). We used the following four statistical indicators as revealed in Table 2, and the result shows that the reference precipitation data of the Climate Hazards Group Infrared Precipitation with Stations (CHIRPS) (NSE = 0.78, Index Of Agreement (D) = 0.94, RMSE = 28.29, Pearson coefficient (CC) = 0.98 and Maximum temperature of European Community Medium-range Weather Forecasts v5 (ECMWFERA5), ERA5 (NSE = 0.81, Index Of Agreement (D = 0.94, RMSE = 0.75 and Pearson coefficient (CC) = 0.96 have very good performance against the basin observed data as shown in Table 2. The mean monthly precipitation spatial variation of CHIRPS data shows overestimation of southwestern data and under estimation of some central parts compared to the ground observed data as shown in Figure 2a. Similarly, Figure 2b indicates that the spatial variation of maximum temperature with overestimation in central and northern region of the basin related to the maximum temperature observed data.

Table 2. Gridded dataset of maximum temperature and precipitation evaluation with Omo River Basin observed data.

Mean Monthly Gridded Data	CHIRPS	CGCC	CPC	ERA5	CRU
		Precipitation (mm)			
NSE	0.78	0.04	0.12	0.29	−1.84
D	0.94	0.68	0.77	0.83	0.34
RMSE	28.29	59.35	56.81	48.45	102.34
Pearson coefficient (CC)	0.98	0.43	0.98	0.73	−0.18
		Temperature (°C)			
NSE			0.13	0.81	−0.01
D			0.81	0.95	0.77
RMSE			1.61	0.75	1.72
Pearson coefficient (CC)			0.97	0.94	0.83

3.2. Evaluation Performance and Ranking of GCMs -CMIP6 Models

After the extraction of precipitation and temperature data, the evaluation performance of 20 CMIP6 models were carried out against the reference data set of mean monthly precipitation (CHIRPS) and temperature (ERA5) for 1985–2014 using Multicriteria Decision Making (MCDM) techniques of compromising programming. For evaluation of the models, five indicators' metrics such as: Nash–Sutcliff efficiency (NSE), percent of bias (PBIAS %), normalized root mean square error (NRMSE), skill score (SS) and correlation coefficient (CC) were used and the models ranking have been performed based on statistical metrics indicators and ideal values (Lp). Accordingly, the results demonstrate that, as shown in Table 3, the GFDL-CM4, NorESM2-MM, CanESM5, NorESM2-LM, and GFDL-ESM4 have the best performance to replicate precipitation. The performance of the 20-model ensemble and the top 3 CMIP6 ensemble models has been assessed here and contrasted to that of a single climate model. When compared to the GFDL-CM4 model, both the ensemble of 20 GCMs and the ensemble of the best 3 models in Table 3 exhibit slightly better performance in reproducing the precipitation over the Omo River Basin. The NorESM2-MM, MPI-ESM1-2-LR, CMCC-ESM2, INM-CM5, BCC-CSM2-MR, NorESM2-LM, and INM-CM4-8 models exhibit the best results among the 20 models for simulating maximum temperature, as shown in Table 4. Regarding this, the NorESM2-MM model exhibits outstanding performance compared to the top 3 ensemble models and 20 ensemble models, and has been selected to replicate the basin's maximum temperature in the future. In contrast, some models such as the MIROC6, CanESM5, and NESM3 models have shown to poorly reproduce the precipitation, whereas the KIOST-ESM, KACE-1-0-G, and IPSL-

CM6A-LR models have shown least performance in respective order to replicate maximum temperature over Omo River Basin.

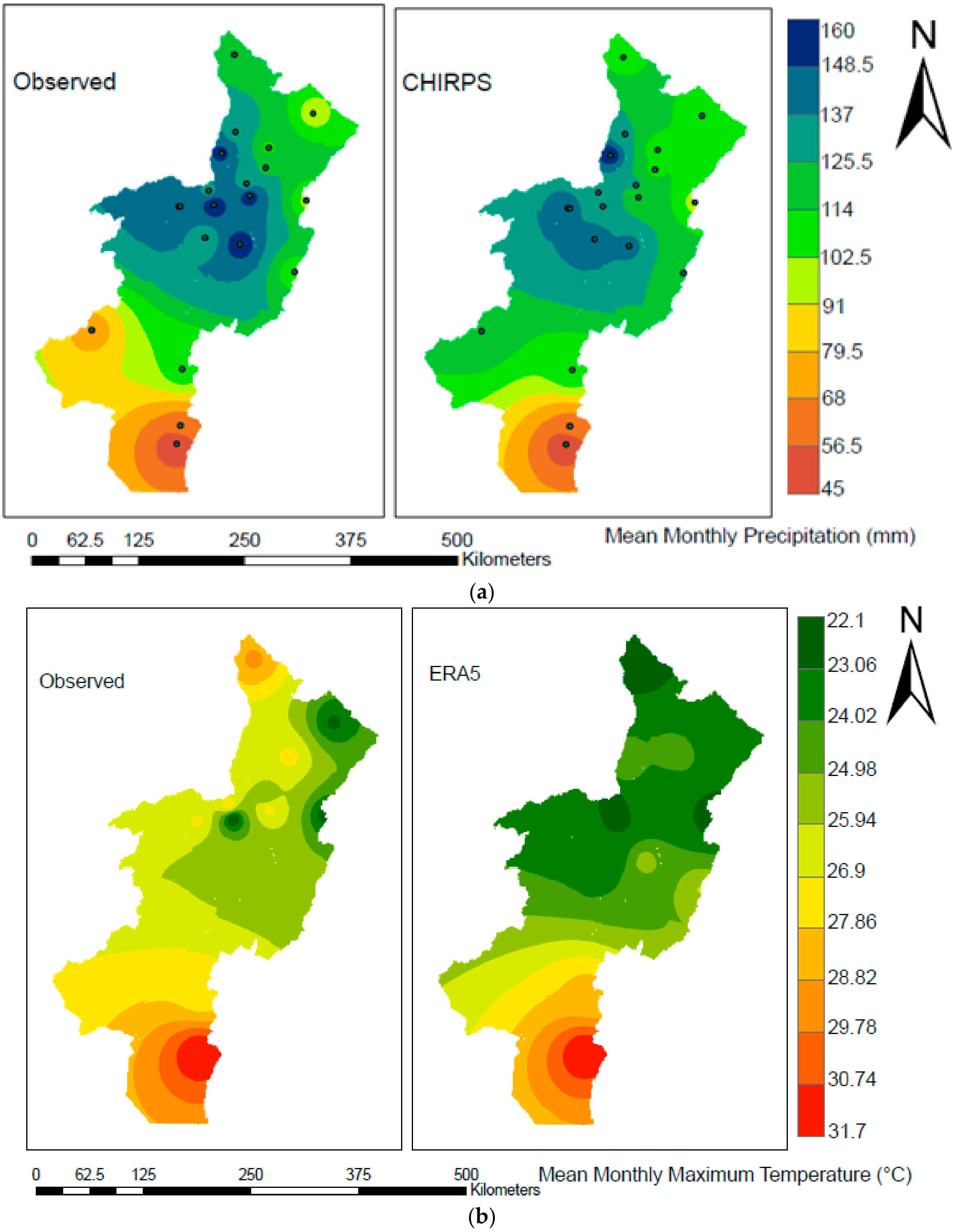

Figure 2. Mean monthly spatial variation of precipitation (CHIRPS) (**a**) and maximum temperature (ERA5) (**b**) against average observed data over the Omo River Basin.

Table 3. Statistical indicators and ranking of precipitation GCMs CMIP6 models using CP technique.

	GCMs	NSE	Pbias	SS	NRMSE	CC	Lp Value	Rank
1	ACCESS-CM2	0.36	0.07	0.05	0.03	0.02	0.54	18
2	ACCESS-ESM1-5	1.09	0.12	0.03	0.03	0.04	1.31	21
3	BCC-CSM2-MR	0.41	0.07	0.03	0.01	0.00	0.53	17
4	CanESM5	0.08	0.03	0.03	0.01	0.01	0.15	5
5	CMCC-ESM2	0.41	0.06	0.04	0.03	0.06	0.60	20
6	GFDL-CM4	0.06	0.02	0.04	0.00	0.00	0.13	3
7	GFDL-ESM4	0.15	0.02	0.03	0.01	0.01	0.21	7
8	INM-CM4-8	0.38	0.12	0.03	0.02	0.01	0.57	19
9	IPSL-CM6A-LR	0.28	0.06	0.03	0.02	0.02	0.41	11
10	INM-CM5-0	0.39	0.07	0.01	0.01	0.01	0.49	16
11	KACE-1-0-G	0.19	0.00	0.10	0.09	0.09	0.46	14
12	KIOST-ESM	0.20	0.06	0.05	0.03	0.09	0.44	13
13	MIROC6	1.61	0.20	0.03	0.03	0.00	1.87	22
14	MPI-ESM1-2-HR	0.19	0.05	0.05	0.02	0.01	0.32	10
15	MPI-ESM1-2-LR	0.15	0.06	0.03	0.02	0.00	0.26	9
16	MRI-ESM2-0	0.16	0.05	0.00	0.01	0.01	0.22	8
17	NESM3	0.28	0.06	0.04	0.03	0.01	0.43	12
18	NorESM2-LM	0.07	0.03	0.05	0.01	0.00	0.16	6
19	NorESM2-MM	0.07	0.02	0.04	0.00	0.00	0.14	4
20	TaiESM1	0.36	0.04	0.04	0.01	0.02	0.47	15
	All Ensemble	0.05	0.02	0.03	0.00	0.00	0.10	2
	Top3Ensemble	0.00	0.00	0.04	0.00	0.00	0.05	1

Table 4. Statistical indicators and ranking of maximum temperature GCMs CMIP6 using CP technique.

	GCMs	NSE	Pbias	SS	NRMSE	Person	Lp Value	Rank
1	ACCESS-CM2	1.08	0.01	0.04	0.00	0.03	1.16	16
2	ACCESS-ESM1-5	0.56	0.00	0.03	0.00	0.04	0.63	9
3	BCC-CSM2-MR	0.46	0.00	0.03	0.00	0.00	0.49	8
4	CanESM5	2.43	0.01	0.04	0.00	0.02	2.51	19
5	CMCC-ESM2	0.16	0.00	0.04	0.00	0.01	0.21	5
6	GFDL-CM4	1.05	0.01	0.05	0.00	0.01	1.12	15
7	GFDL-ESM4	0.86	0.01	0.05	0.00	0.02	0.94	13
8	INM-CM4-8	0.59	0.01	0.05	0.00	0.01	0.66	10
9	INM-CM5	0.32	0.01	0.04	0.00	0.00	0.37	6
10	IPSL-CM6A-LR	3.20	0.02	0.08	0.00	0.03	3.33	20
11	KACE-1-0-G	4.92	0.02	0.09	0.00	0.08	5.12	21
12	KIOST-ESM	16.01	0.04	0.07	0.01	0.01	16.12	22
13	MIROC6	2.43	0.02	0.05	0.00	0.00	2.50	18
14	MPI-ESM1-2-HR	0.95	0.01	0.04	0.00	0.02	1.02	14
15	MPI-ESM1-2-LR	0.16	0.00	0.01	0.00	0.01	0.18	3
16	MRI-ESM2-0	0.62	0.01	0.04	0.00	0.03	0.70	11
17	NESM3	1.96	0.01	0.08	0.00	0.03	2.08	17
18	NorESM2-LM	0.46	0.01	0.01	0.00	0.00	0.48	7
19	NorESM2-MM	0.00	0.00	0.02	0.00	0.00	0.02	1
20	TaiESM1	0.78	0.01	0.05	0.00	0.01	0.85	12
	All Ensemble	0.17	0.00	0.03	0.00	0.01	0.20	4
	Top3Ensemble	0.06	0.00	0.00	0.00	0.00	0.06	2

3.3. Spatial Evaluation of GCMs with CHIRPS Precipitation

The spatial variation skill of mean monthly precipitation of 20 GCMs CMIP6 models was appraised using CHIRPS data over the period of 1985–2014. The performance variation of the CMIP6 models in their abilities to replicate the CHIRPS precipitation was observed as shown in Figure 3. Nonetheless, nearly all GCMs exhibit comparable characteristics in some areas, such as lower precipitation in the southern and somewhat central region of the basin. On other hand, the INM-CM4-8, INM-CM5, IPSL-CM6A-LR, ACCESS-CM2, BCC-CSM2-MR, and TaiESM1 models display overestimation over the basin. In contrast, the ACCESS-CM2, NorESM2-LM, KIOST-ESM, NESM3, MPI-ESM1-2-HR, and MPI-ESM1-2-LR models indicate the underestimation of precipitation through the region. On other hand, the MIROC6, ACCESS-ESM1-5, and MRI-ESM2-0 models reveal a high overestimation of mean monthly precipitation in the northern and central part of the basin. The remaining climate models including ensemble models detect good performance relatively.

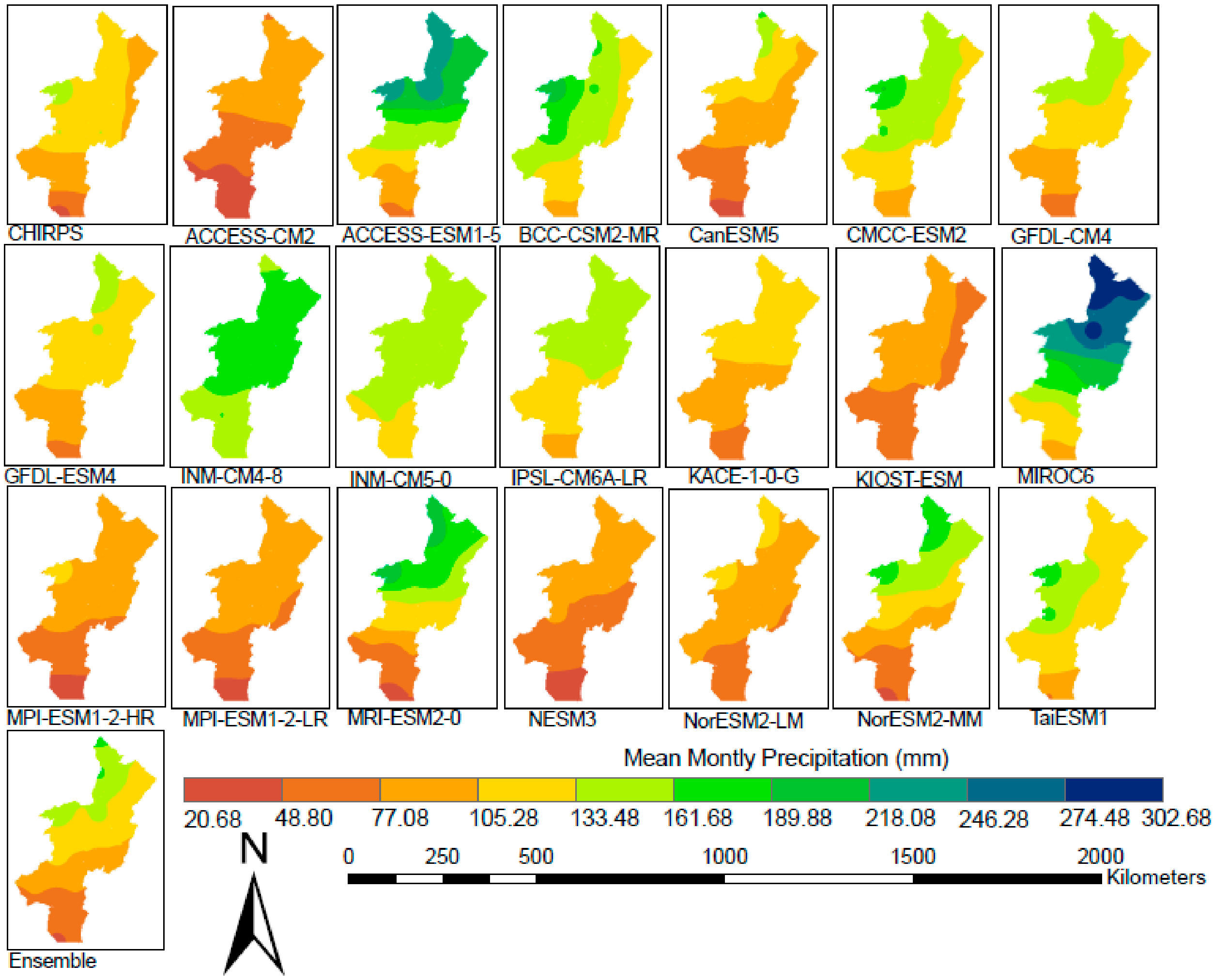

Figure 3. Spatial Evaluation of GCMs with CHIRPS precipitation.

3.4. Spatial Evaluation of GCMs with ERA5 Maximum Temperature

Figure 4 illustrates how well the 20 GCMs CMIP6 models replicated the ERA5 mean monthly maximum temperature spatially. The outcome demonstrates that models simulated an overestimation of the maximum temperature especially in the northern areas, and underestimations in southern areas of the basin. On the other hand, underestimation of the maximum temperature was detected compared to ERA5 by some models such as KACE-1-0-G, KIOST-ESM, and CanESM5 in the southern, central, and northern areas of the basin region. Furthermore, the GFDL-ESM4, GFDL-CM4, IPSL-CM6A-LR, and NESM3 models indicate the overestimation of the maximum temperature over the basin. Comparatively, the remaining CMIP6 models including ensemble models replicate the maximum temperature of the ERA5 throughout the basin.

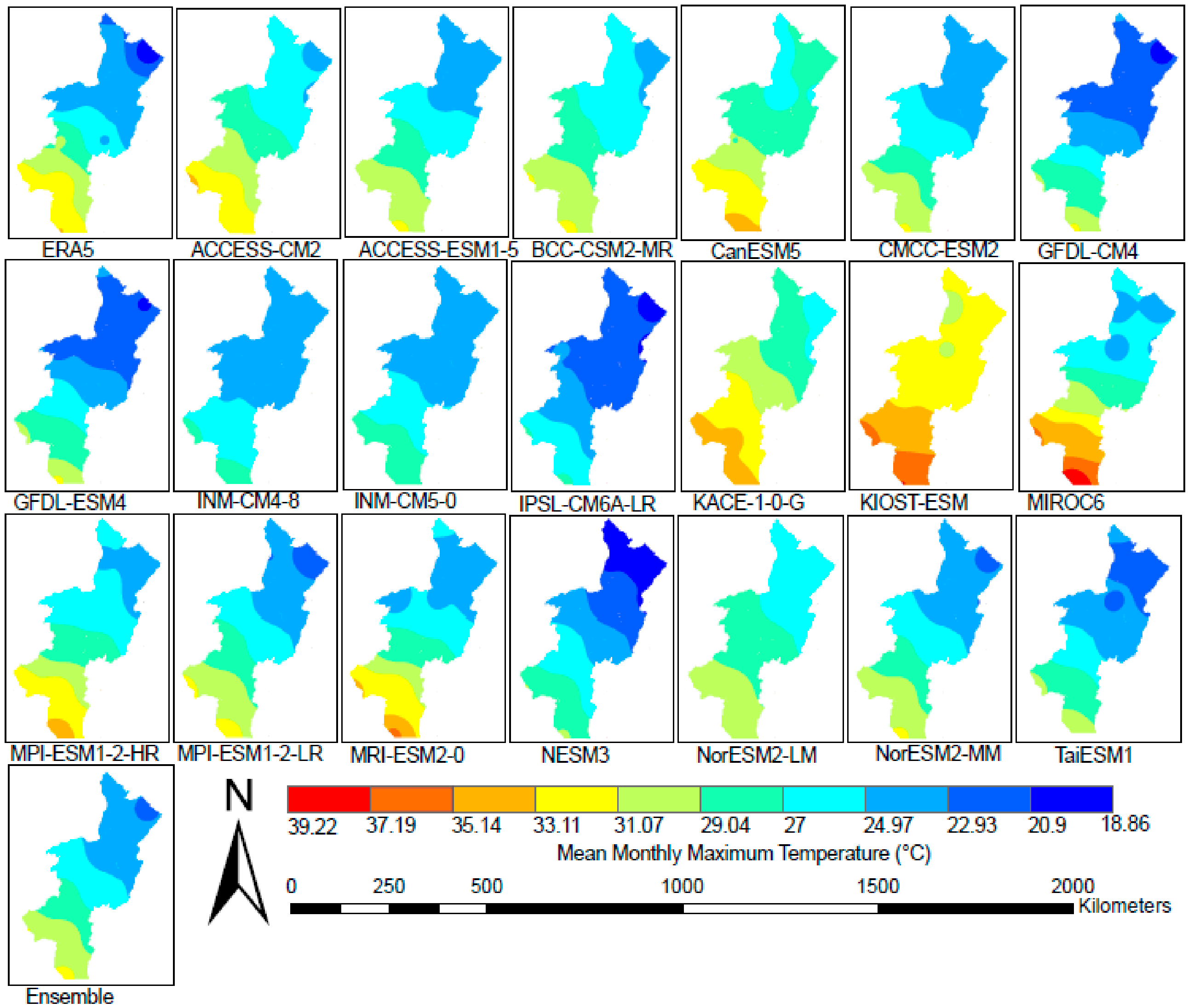

Figure 4. Spatial Evaluation of GCMs with ERA5 Maximum Temperature.

3.5. Taylor Diagram

The Taylor diagram was applied in this study to assess how well the GCMs models performed in terms of their correlation, their root-mean-square difference, and their ratio of standard deviation, and it was found that all three could be plotted simultaneously. Accordingly, the performance of the mean monthly precipitation and maximum temperature GCMs were relative to reference data as shown in Figure 5a,b, respectively. The result indicates that the GFDL-CM4, MPI-ESM1-2-LR, NorESM2-LM NorESM2-MM, CanESM5, and MPI-ESM1-2-HR models have performed well, having less distance from the precipitation reference data. Furthermore, the ensemble models show very good performance next to the MPI-ESM1-2-LR model. On other hand, some of the CMIP6 models such as the KIOST-ESM, ACCESS-CM2, and TaiESM1 models have shown poor performance compared to the others. In the case of the maximum temperature, the NorESM2-MM, NorESM2-LM, INM-CM5, and INM-CM4-8 models were close to the reference maximum temperature and have been shown good performance, whereas the ACCESS-CM2, ACCESS-ESM1-5, and MPI-ESM1-2-HR models have shown poor skill related to the others. The ensemble models indicate well performance compared to some climate models.

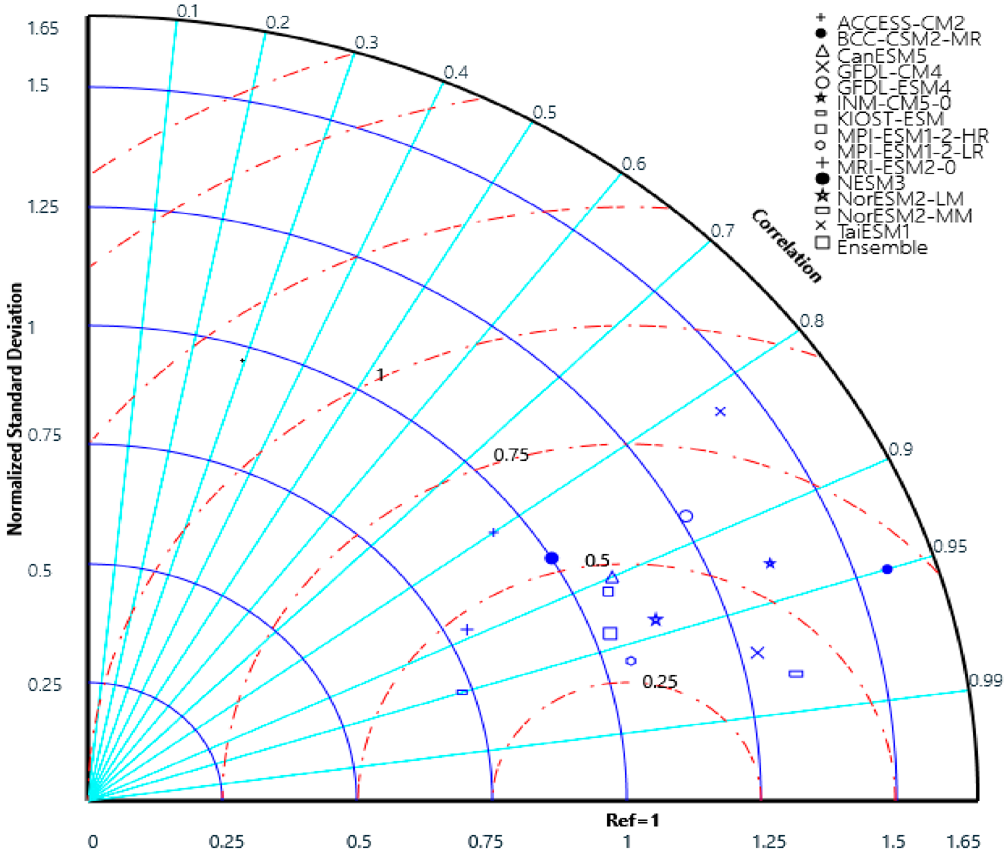

(**a**)

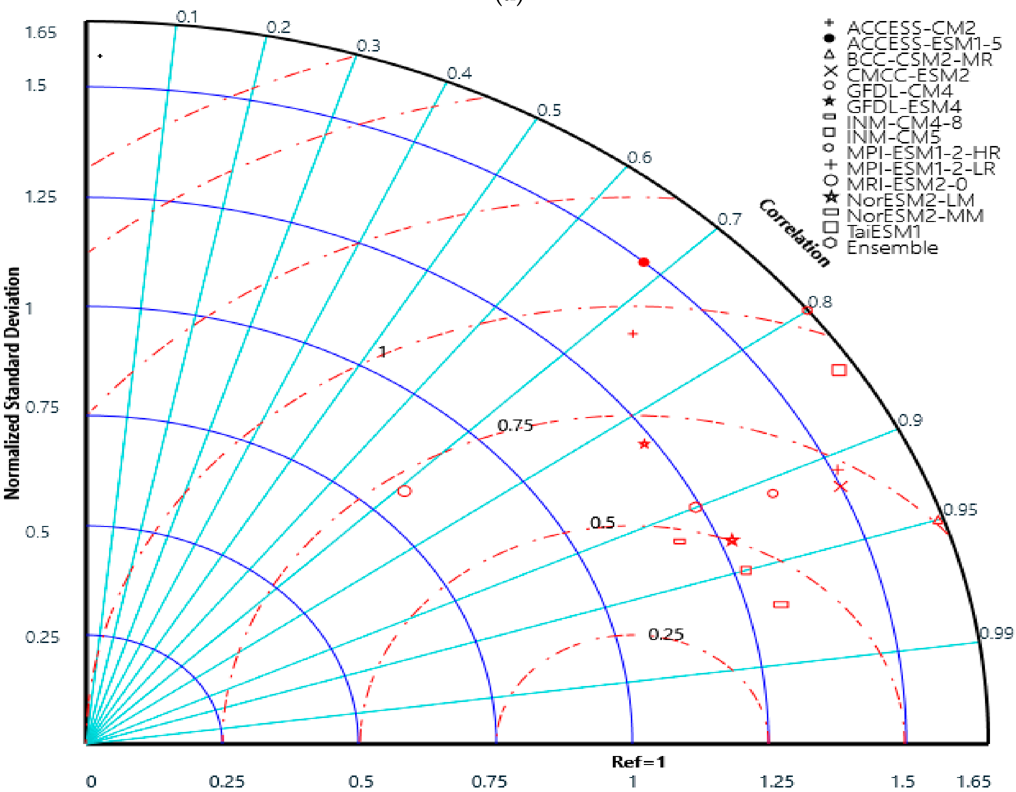

(**b**)

Figure 5. Taylor diagram showing the correlation of GCM with (**a**) precipitation CHIRPS, and (**b**) Maximum Temperature ERA5.

3.6. Assessment of Future Climate Climatology Trend Analysis

The assessment of future precipitation and temperature trend analysis was conducted after downscaling and bias correction for the best-performing models. The nonparametric Mann–Kendall trend test was executed in R studio for SSP245 and SSP585 for the periods of near-future 2031–2060 and far future 2071–2100. The trend analysis was focused on two rainfall seasons of mean annual time series for precipitation and maximum temperature, and the results are presented in Tables 5 and 6. Here, we considered only the top three best-performing climate models and the ensemble of these models for both precipitation and maximum temperature as shown in the Tables 3 and 4, respectively. The CMIP6 GFDL-CM4 precipitation trend test in both rainfall seasons June, July, August and September (JJAS) and March, April, and May (MAM) under the near-future SSP2452031-2060 and SPP5852031-2060 scenarios show positive Z-values or an increasing trend. In the same manner, the trend precipitation of JJAS and MAM under the SSP2452071-2100 and SSP5852071-2100 scenarios indicate an increasing trend except JJAS rainfall seasons as shown below in the Table 5. The CanESM5 precipitation shows an increasing trend in all scenarios except in the scenario of the SSP2452071_2100 scenario in JJAS season. However, the NorESM2-MM precipitation shows a decreasing trend in the seasons of MAM for the SSP2452031-2060 scenario and JJAS for SSP5852031-2060 and SSP5852071-2100 scenarios. The ensemble models trend analysis shows an increasing trend in JJAS season under the SSP2452031-2060, SSP5852031-2060, and SSP5852071-2100 scenarios with Z and p- values of 2.14, 0.03, 2.18, 0.03, and 1.11, 0.27, respectively. However, a decreasing trend was detected in JJAS season under SSP2452071-2100 scenario with a Z value of -1.21 and a p value of 0.23. The positive Z-value was detected in both JJAS and MAM seasons under all scenarios as shown in the Table 5. The ensemble projected seasonal precipitation of JJAS over the Omo River Basin, showing that increasing trend with 99, 89, and 85 mm per year under the SSP2452031-2060, SSP5852031-2060, and SSP5852071-2100 scenarios respectively, except for a decreasing trend in the JJAS season for the SSP2452071-2100 scenario with 69 mm per year. In the MAM season, the precipitation is expected to increase by 13, 157, 53, and 111 mm per year under the SSP2452031-2060, SSP2452071-2100, SSP5852031-2060, and SSP5852071-2100 scenarios respectively.

The mean annual seasonal time series of the projected precipitation is shown in the Figure 6a–d for two rainfall seasons in the Omo River Basin. The Figure 6a shows overestimation of the models in both JJAS and MAM seasons except for the underestimation of NorESM2-MM in both seasons under SSP2452031-2060. Under the SSP24571-2100 scenario, the models show an overestimation of precipitation in both seasons except for the underestimation of GFDL-CM4 in the MAM season and the NorESM2-MM model in the JJAS season. Almost all the models indicate an overestimation in the MAM season in Figure 6c and the NorESM2-MM model shows an underestimation in both seasons in Figure 6d.

The mean annual seasonal maximum temperature trend test of the CMIP6 NorESM2-MM, MPI-ESM1-2-LR, CMCC-ESM2 models and their ensemble was executed as presented in the Table 6, and Figure 7a–d for the JJAS and MAM seasons. The projected average annual maximum temperature time series of the top three best models show an increasing trend in both seasons except for a decreasing trend in the MAM season by NorESM2-MM under the SSP24571-2100 scenario. The projected maximum temperature of the ensemble reveals an increasing trend in JJAS with Z values of 2.08, 1.38, 2.58, and 3.58 and p values of 0.14, 0.24, 0.02, and 0.00 under near-future scenarios SSP2452031-2060 and SSP5852031-2060, and far-future scenarios SSP2452071-2100 and SSP5852071-2100, respectively. The Z-value and P-value of the best selected model of NorESM2-MM are presented in the Table 6. The projected maximum temperature that will be increased over the Omo River Basin in average are 0.95, 1.78, 1.4, and 3.88 °C in JJAS and 1.53, 2.24, 1.56, and 3.89 °C in MAM under climate change scenarios of near-future SSP2452031-2060, SSP5852031-2060, and far-future SSP2452071-2100 and SSP5852071-2100, respectively.

Table 5. Mann–Kendall trend test result of precipitation.

GFDL-CM4-Precipiatation (mm)	Z	p	CanESM5-Precipiatation (mm)	Z	p
SSP2452031_2060-JJAS	0.07	0.94	SSP2452031_2060JJAS	2.14	0.03
SSP2452031_2060-MAM	0.18	0.86	SSP2452031_2060MAM	0.11	0.91
SSP2452071_2100-JJAS	−0.07	0.94	SSP2452071_2100JJAS	−1.21	0.23
SSP2452071_2100-MAM	1.00	0.32	SSP2452071_2100MAM	1.86	0.06
SSP5852031_2060-JJAS	1.71	0.09	SSP5852031_2060JJAS	2.18	0.03
SSP5852031_2060-MAM	1.78	0.07	SSP5852031_2060MAM	0.86	0.39
SSP5852071_2100-JJAS	1.39	0.16	SSP5852071_2100JJAS	1.11	0.27
SSP5852071_2100-MAM	1.14	0.25	SSP5852071_2100MAM	1.61	0.11
NorESM2-MM-Precipiatation (mm)			**Ensemble**		
SSP2452031_2060JJAS	0.11	0.91	SSP2452031_2060JJAS	0.77	0.63
SSP2452031_2060MAM	−0.04	0.97	SSP2452031_2060MAM	0.08	0.91
SSP2452071_2100JJAS	0.36	0.72	SSP2452071_2100JJAS	−0.31	0.63
SSP2452071_2100MAM	2.14	0.03	SSP2452071_2100MAM	1.67	0.14
SSP5852031_2060JJAS	−0.82	0.41	SSP5852031_2060JJAS	1.02	0.18
SSP5852031_2060MAM	0.11	0.91	SSP5852031_2060MAM	0.92	0.46
SSP5852071_2100JJAS	−0.46	0.64	SSP5852071_2100JJAS	0.68	0.36
SSP5852071_2100MAM	0.79	0.43	SSP5852071_2100MAM	1.18	0.26

Table 6. Mann–Kendall trend test result of maximum temperature.

NorESM2-MM-Temperature (°C)	Z	p	MPI-ESM1-2-LR-Temperature (°C)	Z	p
SSP2452031_2060JJAS	3.07	0.00	SSP2452031_2060JJAS	0.86	0.39
SSP2452031_2060MAM	1.82	0.07	SSP2452031_2060MAMM	0.71	0.48
SSP2452071_2100JJAS	0.89	0.37	SSP2452071_2100JJAS	1.00	0.32
SSP2452071_2100MAM	−0.79	0.43	SSP2452071_2100MAM	0.79	0.43
SSP5852031_2060JJAS	2.71	0.01	SSP5852031_2060JJAS	1.86	0.06
SSP5852031_2060MAM	1.39	0.16	SSP5852031_2060MAM	1.32	0.19
SSP5852071_2100JJAS	3.85	0.00	SSP5852071_2100JJAS	2.71	0.01
SSP5852071_2100MAM	2.43	0.02	SSP5852071_2100MAM	1.43	0.15
CMCC-ESM2-Temperature (°C)			**Ensemble**		
SSP2452031_2060JJAS	2.32	0.02	SSP2452031_2060JJAS	2.08	0.14
SSP2452031_2060MAM	2.21	0.03	SSP2452031_2060MAM	1.58	0.19
SSP2452071_2100JJAS	2.25	0.02	SSP2452071_2100JJAS	1.38	0.24
SSP2452071_2100MAM	1.14	0.25	SSP2452071_2100MAM	0.38	0.37
SSP5852031_2060JJAS	3.18	0.00	SSP5852031_2060JJAS	2.58	0.02
SSP5852031_2060MAM	1.61	0.11	SSP5852031_2060MAM	1.44	0.15
SSP5852071_2100JJAS	4.17	0.00	SSP5852071_2100JJAS	3.58	0.00
SSP5852071_2100MAM	3.50	0.00	SSP5852071_2100MAM	2.45	0.06

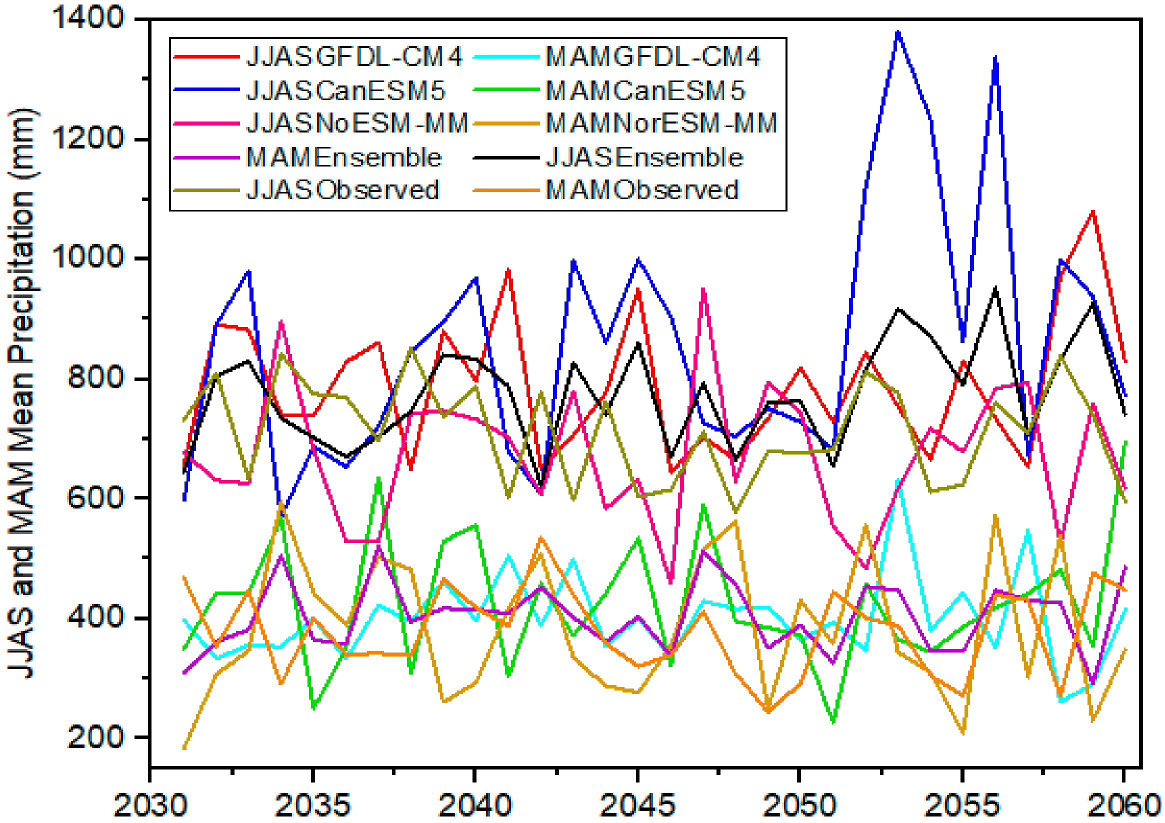

(a)

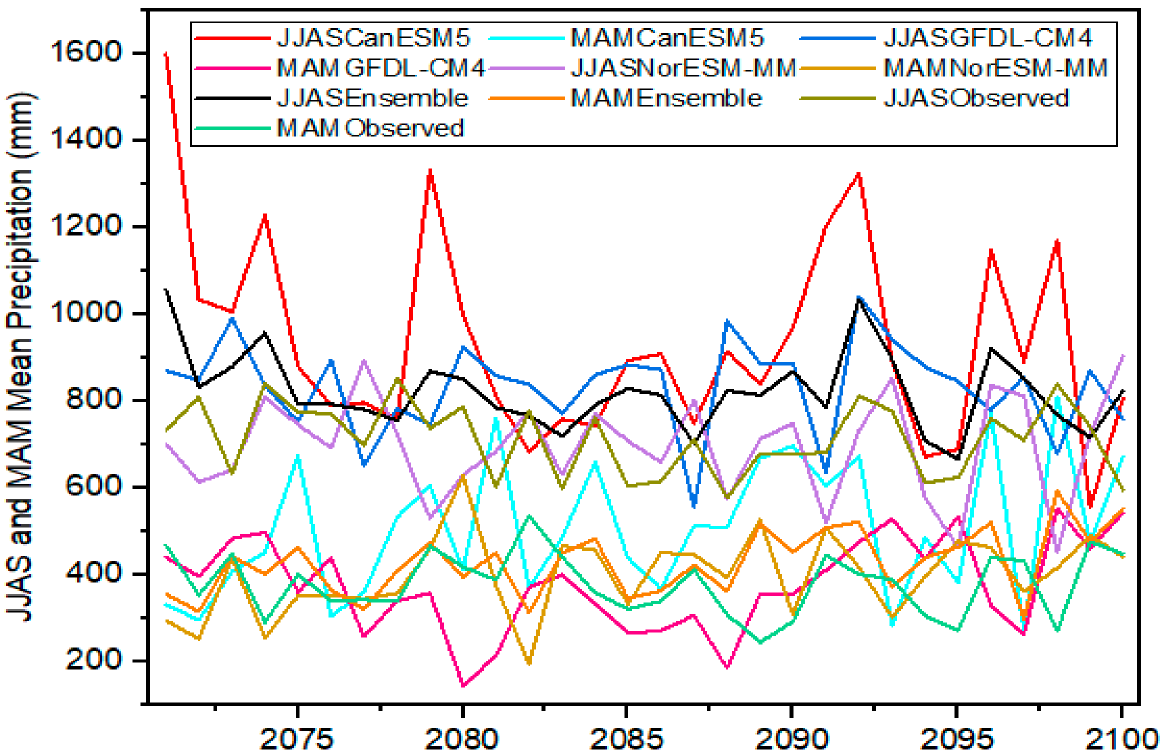

(b)

Figure 6. *Cont.*

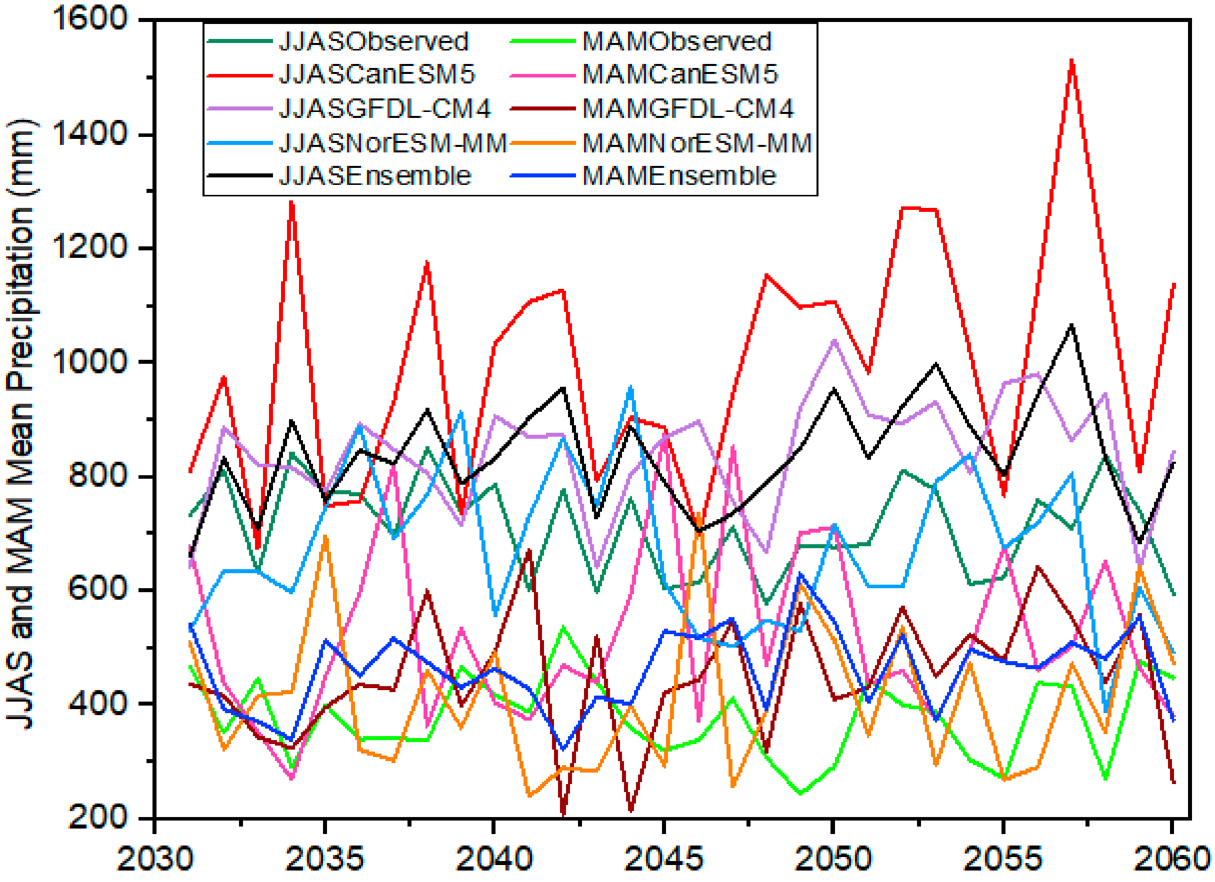

(**c**)

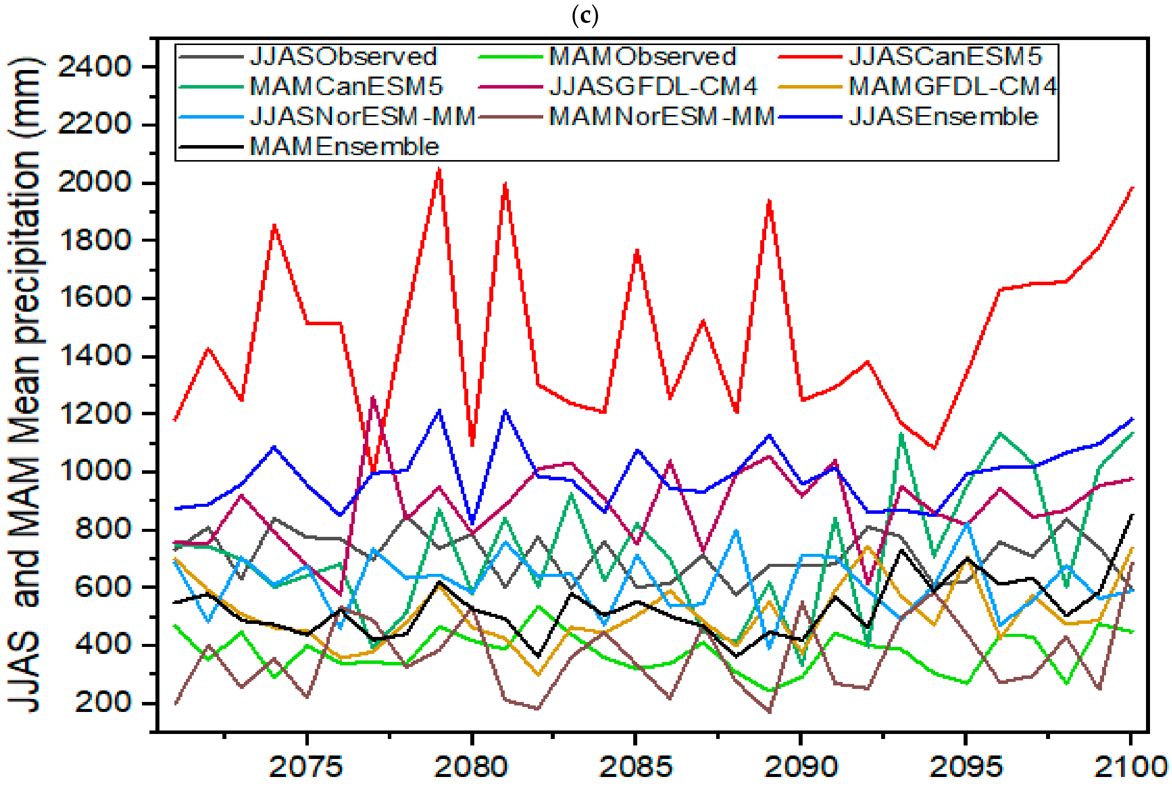

(**d**)

Figure 6. Projected mean precipitation of JJAS and MAM (**a**) SSP2452031-2060, (**b**) SSP2452071-2100, (**c**) SSP5852031-2060, and (**d**) SSP5852071-2100 with observed data.

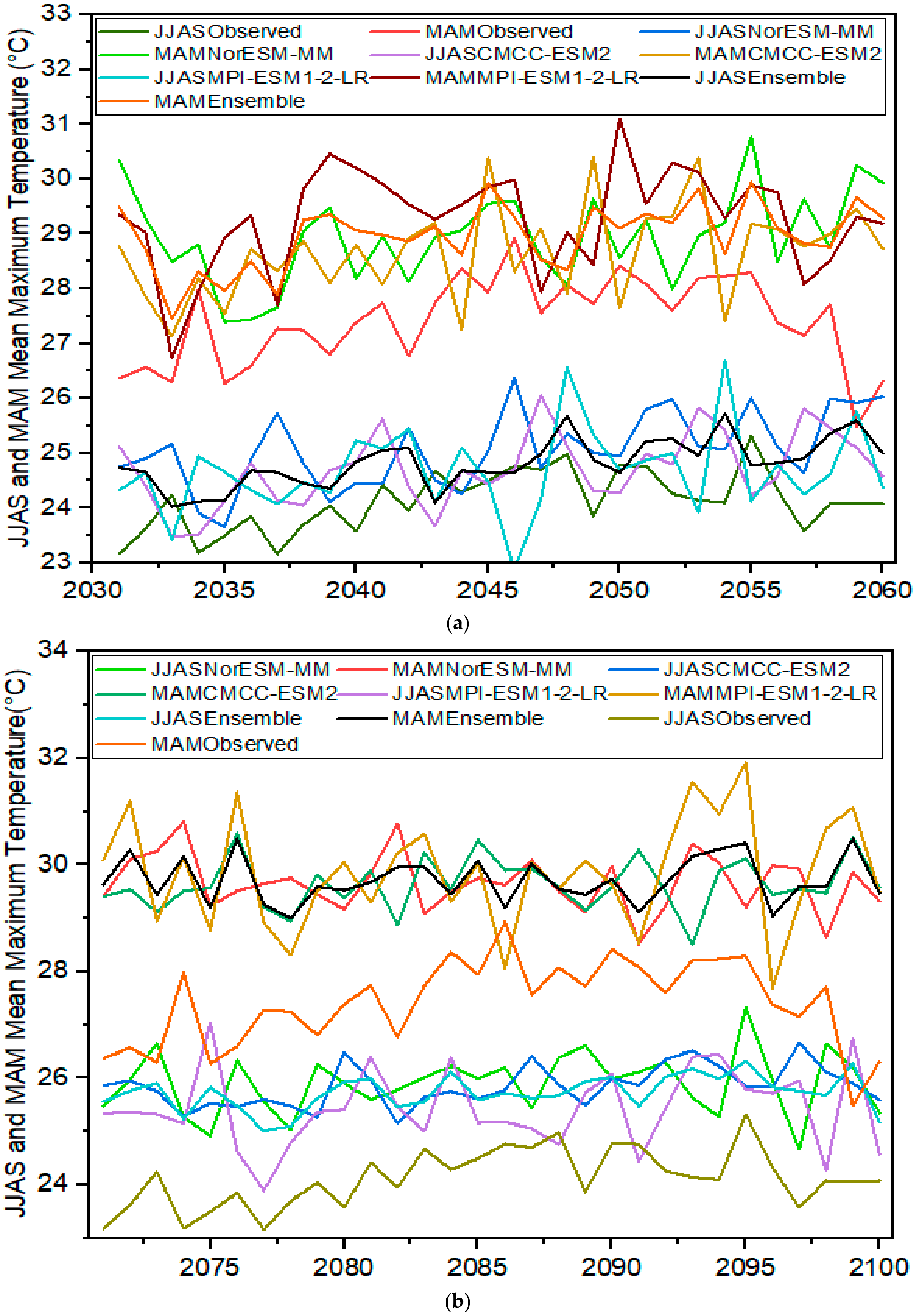

Figure 7. *Cont.*

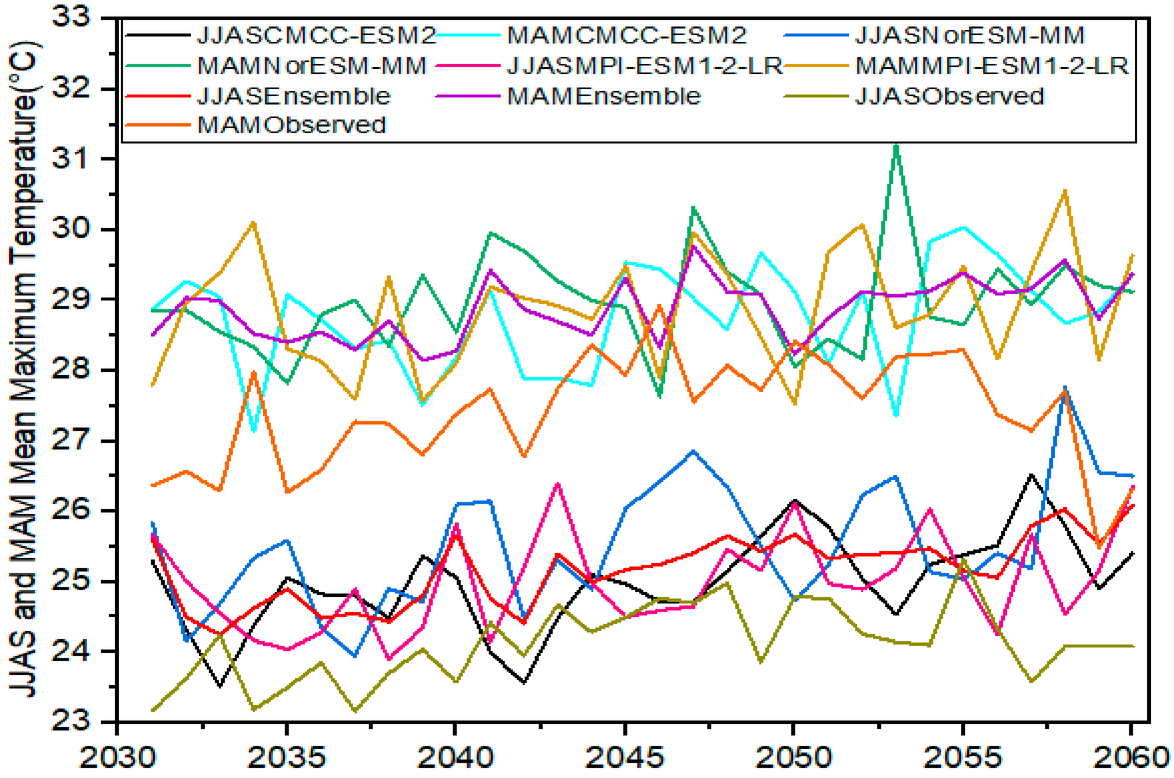

(**c**)

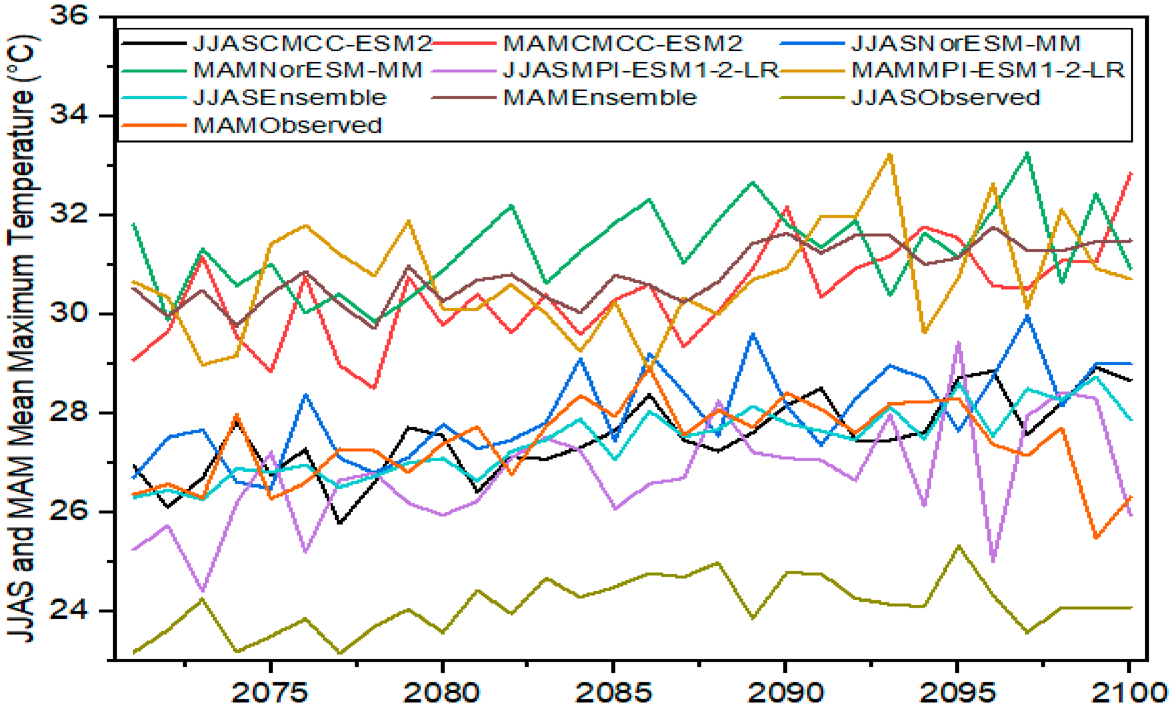

(**d**)

Figure 7. Projected mean maximum temperature of JJAS and MAM (**a**) SSP2452031-2060, (**b**) SSP2452071-2100, (**c**) SSP5852031-2060, and (**d**) SSP5852071-2100 with observed data.

The graphs of the top three best models of maximum temperature and their ensemble show overestimation and captured well the trend of observed data compared to precipitation models as shown in the Figure 7a–d.

3.7. Spatial Variation of Future Climate Change

Figure 8a shows how the mean monthly precipitation from June to September is distributed spatially for both near and far-future scenarios using the SSP245 and SSP585 scenarios. Under all possible scenarios, the southern Omo River Basin region experiences lower mean monthly precipitation (31.87–169.4 mm) than the other regions of the basin in rainy season of JJAS. In contrast, a higher magnitude of precipitation (215.24–352.77 mm) is observed over the northwestern part of the region under all scenarios and central regions under scenario SSP585, especially under the SSP5852071-2100 scenario. Particularly, the precipitation is overestimated in the central and northern areas in all scenarios, except by the NorESM2-MM model and even overstimulated the basin by CanESM5 model under the SSP5852071-2100 scenario. Similarly, the northern and western areas of the basin receive 44.8–130.66 mm precipitation in the MAM season under all near-future scenarios, even more precipitation is expected up to 216.52 mm in the southeastern area under all far scenarios and the SSP5852031-2060 near-future scenario of the CanESM5 model. In this season, the central region receives more precipitation from 130.66–273.76 mm under different scenarios, and even more precipitation up to 331 mm under the SSP5852071-2100 scenario of the CanESM5 model. Generally, the average spatial distribution of the mean monthly precipitation over the basin indicates an increasing pattern in JJAS from 15.17–27.73 mm under the near- and far-future of the SSP245 scenario and from 31.2–69.49 mm under the near- and far-future of the SSP585 scenario. Furthermore, the average spatial precipitation increasing trend is expected in MAM from 8.06–17.12 mm under the SSP245 scenario and from 27.97–51.48 mm under the SSP585 scenario. However, the spatial decreasing trend of precipitation is observed over a few parts of the basin in both seasons under all scenarios except under the SSP5852071-2100 scenario.

Similarly, the projected mean monthly maximum temperature spatial distribution were carried out over the basin for the 2031–2060 and 2071–2100 periods under both scenarios of SSP245 and SSP585 as revealed in Figure 8c. The result displays that the mean monthly maximum temperature in JJAS varies from 20.31–26.56 °C in the northeastern and central part of the basin under near- and far-future scenarios, except for a higher temperature up to 29.7 °C under the far-future SSP5852071-2100 scenarios. In the south and northwestern boundaries of basin, the projected maximum temperature in MAM varies from 28.13–35.96 °C under both scenarios. However, the maximum temperature is expected in MAM to be 26.56–29.7 °C in the central areas, even up to 34.39 °C under the SSP5852071-2100 scenario. In general, the variations of the NorESM2-MM model mean that the monthly maximum temperature simulation over the basin is 0.95–3.88 °C in JJAS and 1.4–3.77 °C in MAM under the stated scenarios.

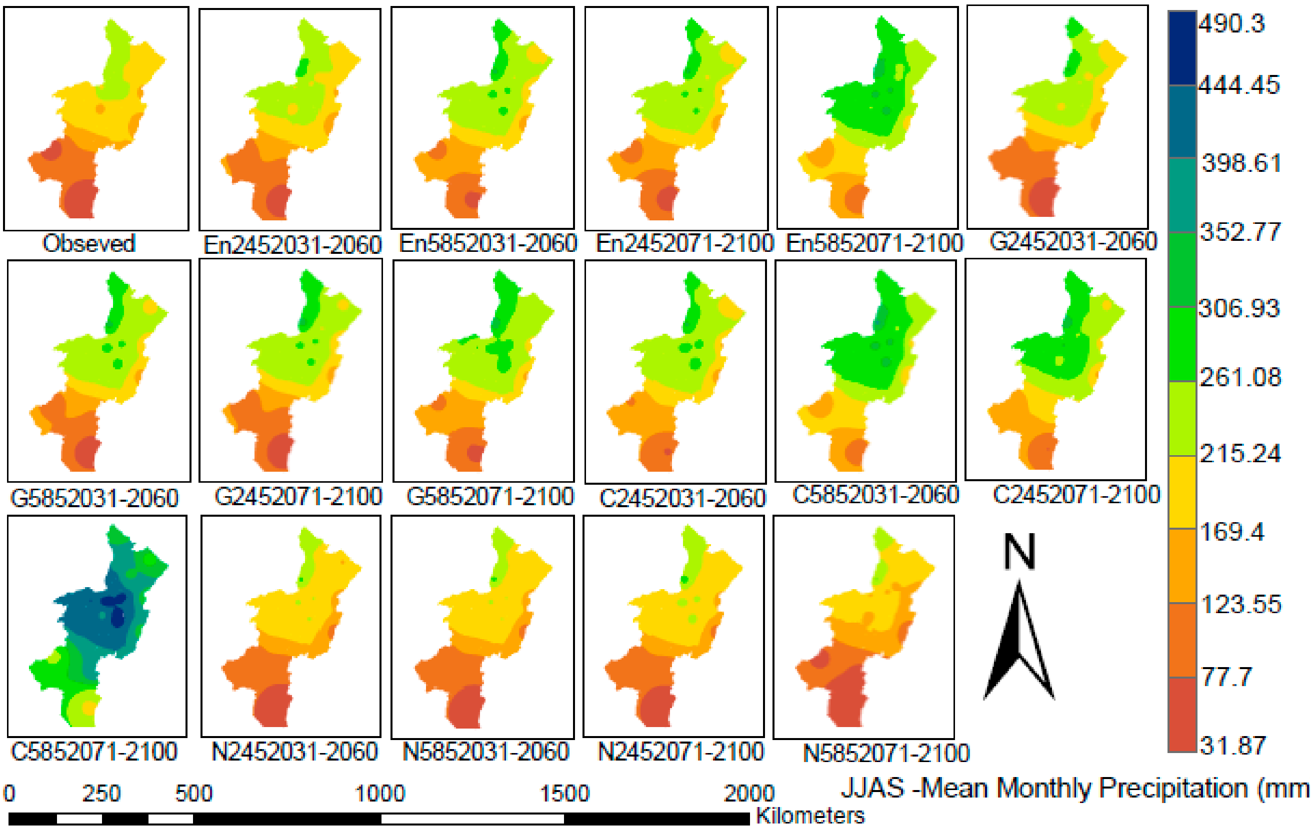

(**a**)

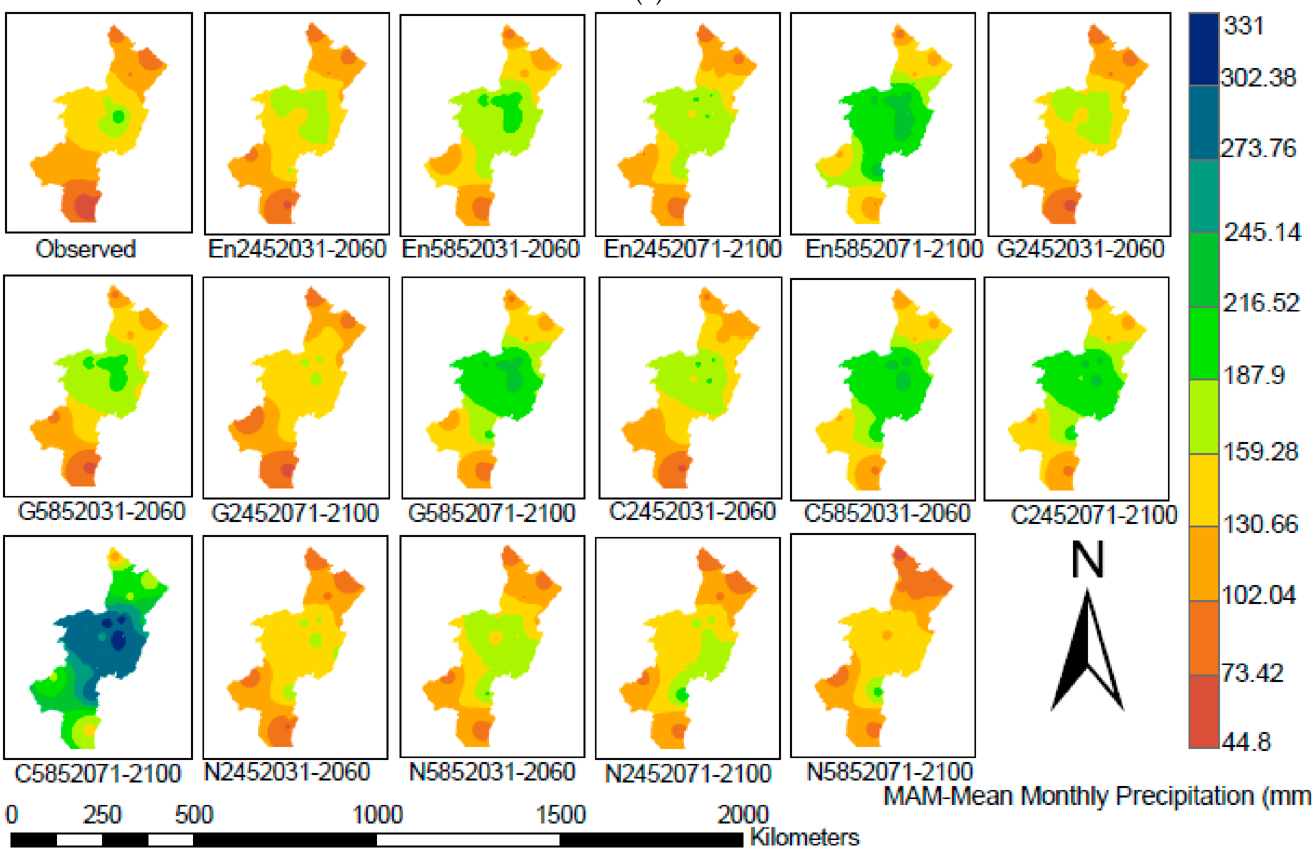

(**b**)

Figure 8. *Cont.*

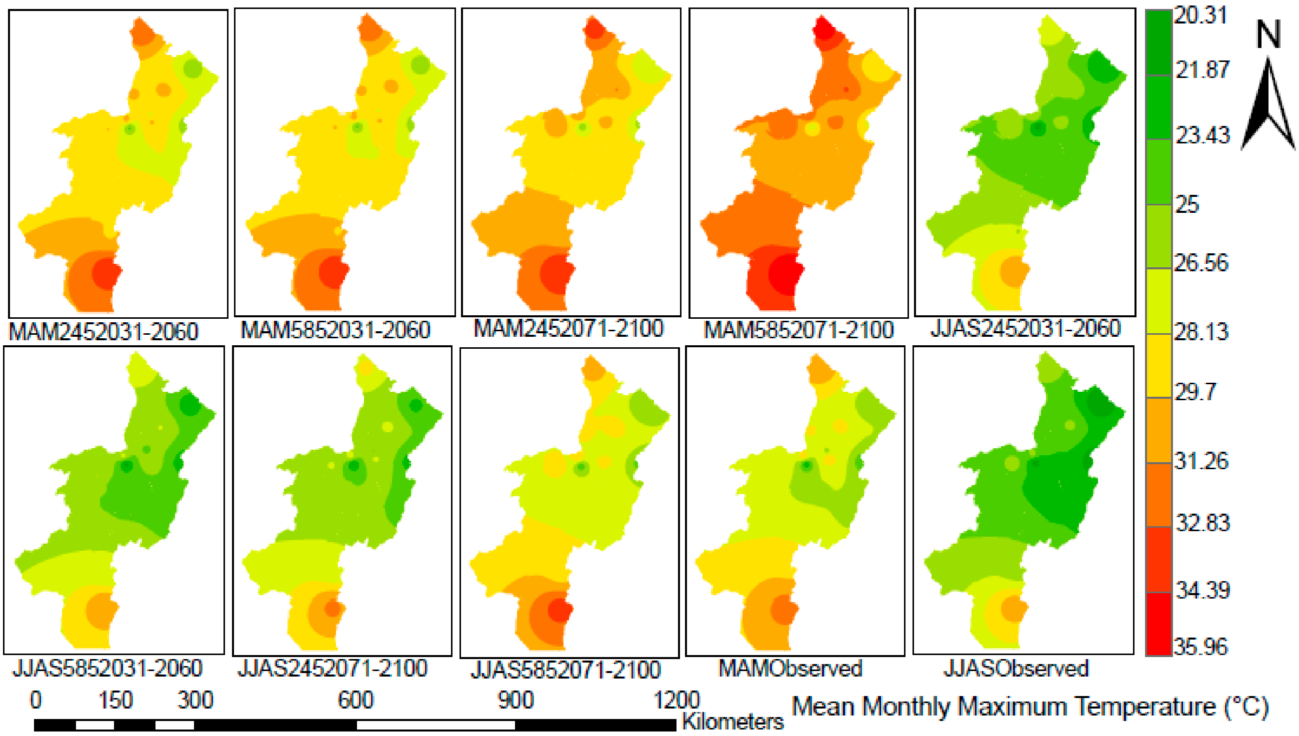

(**c**)

Figure 8. Spatial variation of projected precipitation of (**a**) in JJAS, (**b**) in MAM and (**c**) NorESM2-MM maximum temperature in JJAS and MAM corresponding to SSP scenarios with Observed over the basin. Note: En = Ensemble in JJAS for (**a**), in MAM for (**b**), G = GFDL-CM4, C = CanESM5, and N = NorESM2-MM in both (**a**,**b**).

4. Discussion

4.1. GCMs CMIP6 Models Selection

It is essential for understanding the global climate models created to simulate past climatic conditions and future climate projections in order to identify regional problems and potential solutions in water resource planning and management globally [102]. GCMs are essential for climate projection in countries such as Ethiopia, where the majority of the population depends on rainy season agriculture and has the greatest rates of population growth, necessitating the need for greater water supplies, a resources that is greatly impacted by climate [123]. Because of this, the currently released GCMs CMIP6 model is getting more attention, and scholars have been doing their research in different thematic areas of climate change at global and regional levels [45,49,59,60,62]. On other hand, to reduce the different uncertainties associated with GCM initialization and parameterization [124], spatial variation performances across the globe and the scarcity of observed data for model evaluation, such as gridded datasets, have been utilized to assess the performance of GCMs [14,49,61,125]. In this study, as per the statistical indicator results in Table 2, CHIRPS precipitation and ERA5 maximum temperature gridded datasets show a very good agreement with the average precipitation and maximum temperature observed data, respectively, over the Omo River Basin for the baseline periods of 1985–2014. Proper performance evaluation of CMIP6 models, and further ranking them, is crucial based on their skill to reproduce the observed precipitation and temperatures over the basin to reduce uncertainty produced in different steps [126].

For this study, 20 GCMs CMIP6 have been statistically assessed against reference data sets of precipitation (CHIRPS) and maximum temperature (ERA5) to replicate the observed precipitation and temperature, respectively. A state-of-the-art MCDM approach called compromise programming was used to compromise the performance evaluation metrics of the GCMs for various time frames, as shown in Tables 3 and 4. Accordingly, among 20 CMIP6 models across the basin, the top three best performance model ensembles and NorESM2-MM models performed best in replicating monthly precipitation and maximum temperature, respectively. As a single model, GFDL-CM4 shows the best performance among 20 GCM precipitation models. Previously, researchers have never used multi-CMIP6 models and the MCDM approach, compromising programming for climate studies and models selection in the Omo River Basin. However, very few researchers carried out climate research using GCMs in ensemble approach [18,127]. In contrast, the performance evaluation of CMIP6 models were conducted in Ethiopia; in ref. [62], twelve CMIP6 models were evaluated against GPCC precipitation and ERA5 temperature in the Upper Blue Nile Basin. BCC-CSM-2MR precipitation and MRI-ESM2-0 temperature showed a good agreement with observed datasets. In CMIP6 models of the evaluation of the Awash River Basin, GFDL-CM4, showed good performance in replicating precipitation, but the best performance in simulating minimum temperature [128]. CMIP6 models of precipitation were evaluated against the CHIRPS seasonally and annually over Uganda, and GFDL-CM4 was selected as the best model next to BCC-CM [22]. However, GFDL-CM4 was found to be in third position in model performance assessment in replicating monthly and seasonal rainfall in North Africa [22]. Similarly, GFDL-CM4 has showed good ability in duplicating the observed precipitation in China [129], future projections of temperature and precipitation of Antarctica [130], and the East Asian Meiyu [131]. Ref. [132] conducted the CMIP6 models' performance evaluation using indicators (NSE, PBAIS, and RSR) and NorESM2-MM showed a higher skill for temperature. Although the CMIP6 NorESM2-MM model performs only moderately when simulating summer over the Tibetan Plateau, it performs well when simulating annual temperatures [133]. Ref. [134] assessed the performance of CMIP6 models against ERA5 and NorESM2-MM, and revealed good skill in replicating climatology for the Asian-Pacific region, which validates the result obtained. However, the performances of 12 CMIP6 were assessed against ERA5 in the Upper Blue Nile Basin and MRI-ESM2-0 was selected for temperature; this was due to the research approach followed, complicity of the topography, and climate variation in the basin. Furthermore, ref. [135] selected the NorESM2-MM as the best model to simulate temperature in the evaluation of future water potential and demand for irrigation in the Kankai River Basin, Nepal.

4.2. Bias Correction and Projections of Climate Change Trend Analysis

Currently, the newly released GCMs CMIP6 models have been highly used to simulate and estimate climate change. However, due to their large inherent uncertainty and very coarse resolution, GCMs are not employed directly for climate change impact analysis. The hydrological modeling of future climate change needs understanding of global climate models and emission scenarios, and downscaling of GCMs CMIP6 model output. Regarding making decisions on water resources and environmental management, the accuracy assessment of climate model outputs for temperature and precipitation is very important. Therefore, to reduce the uncertainty in the CMIP6 models, downscaling and bias correction is applied for downscaling to fine resolution at the basin level.

For this study, before future climate change trend analysis, bias correction was performed using the SD GCM tool for baseline periods of 30 years (1985–2014), and near (SSP245/5852031-2060) and far-future (SSP245/5852071-2100) scenarios. Here, we have used three methods, namely Quantile Delta mapping (QDM), Quantile Mapping (QM), and Empirical Quantile Mapping (EQM) to execute the bias correction of CMIP6 models. The daily precipitation and maximum temperature observation data of the basin were used against the model output. To select the most suitable method to reduce uncertainty in the model, three statistical indicators, the Nash–Sutcliff efficiency (NSE), root mean square error (RMSE), and Pearson coefficient (CC) were applied. Based on the result of indicators, the Quantile Delta mapping (QDM) method shows that best performance for precipitation and was applied as the most suitable approach to reduce biases in GCMs CMIP6 models over the Omo River Basin. On other hand, EQM indicates good performance in executing the bias correction in maximum temperature as shown in Table A1 of Appendix A. Furthermore, cumulative density function (CDF) was used for observation and downscaled data based on the most suitable distribution function as shown in the Appendix A Figure A1.

It is crucial to evaluate the seasonal and interannual spatial-temporal variability of precipitation and temperature in a changing climate in order to determine changes caused by the climate and recommend appropriate future water-resource-management methods. Climate change has a severe impact on Ethiopia's socioeconomic structure, particularly in the sectors of hydropower, agriculture, and water supply [136]. This is because of Ethiopia's complicated topographical and geological features, which cause the country's climate to vary greatly in space and have various precipitation patterns [137]. The best CMIP6 models of the top three best performance precipitation model ensembles and NorESM2-MM temperature were used in this work to evaluate future climate projections after bias correction was applied. The evaluation was conducted through visualization of variables' tempo-spatial distribution, and trend assessment.

The result of the top three precipitation models' ensemble trend test in both rainfall seasons JJAS and MAM show an increasing trend under near-future SSP245/5852031-2060 and far-future SPP5852071-2100 scenarios except for a decreasing trend under the far-future SSP2452071-2100 scenario as presented in Table 5. The projected seasonal precipitation of June, July, August, September (JJAS) and March, April, May (MAM) shows an increasing trend with 10.86 and 17.66, 38.96 and 11.85, and 22.1 and 40.7% under SSP2452031-2060, SSP5852031-2060, and SSP5852071-2100 scenarios, respectively. Furthermore, an increasing trend was detected in MAM by 12.8% and a decreasing trend was detected in JJAS by 15.23% under the SSP2452071-2100 scenario. The projected annual maximum temperature time series shows an increasing trend over the Omo River Basin under all scenarios as revealed in Table 5. The maximum temperature projection is to be increased on average by 0.95, 1.78, 1.4, and 3.88 °C in JJAS and 1.53, 2.24, 1.56, and 3.89 °C in MAM under climate change scenarios of near-future SSP2452031-2060 and SSP5852031-2060, and far-future SSP2452071-2100 and SSP5852071-2100, respectively. The pattern change of the projected precipitation and temperature have been conducted by previous researchers using GCM models' output and observed data at different times and regions. For example, ref. [17] used observed data for the period of 1981–2016, and the rainfall trend shows a statistically insignificant positive trend in the northern and central part of the basin in summer and autumn seasons', but a decrease in the southern area and an increasing trend of temperature. Similarly, ref. [18] pointed out the rising tendency of average maximum and minimum temperatures in the future, however the precipitation exhibits a fluctuating trend over the basin under short-term and long-term scenarios. Additionally, the studies in the upper Omo River Basin show that future maximum temperature projection exhibits an increasing trend (1986–2020). However, there was no clear trend, either increasing or decreasing, in the expected precipitation for the years 2021 to 2065 [138]. Ref. [139] performed a non-parametric trend test on monthly data in the upper basin; the findings indicate a rising trend in both precipitation and temperature. In contrast, the projected annual average precipitation decreases from 10.77–13.11% under the RCP 4.5 emission scenario. In this fashion, the study showed a decreasing trend under the RCP 8.5 scenario from 11.10–13.86% in the rainy season from June–August and from March–May of the irregular rain season. On the other hand, under the RCP 4.5 scenario and the RCP 8.5 scenario, the anticipated average temperature rises from 2.40 and 3.34 °C to 2.6 and 4.54 °C, respectively [127]. This study used some of GCMs and ensemble approach, and comes up with the stated results.

However, ref. [128] used 12 GCMs and the CMIP6 model to predict the climate in the Upper Awash Basin for the years 2040–2069. The results indicate an increase in annual precipitation with mean changes of 6.4% for SSP2-4.5 and 10.6% for SSP5-8.5 scenarios. Similar to this, the two scenarios predicted increases in precipitation of 7.9% and 19.7%, respectively, for the years 2070–2099. The average annual maximum temperature shows an increasing trend, with a mean value of 1.6 °C under SSP2-4.5 and 2.0 °C under SSP5-8.5

in 2040–2069. Values of 2.0 °C and 3.0 °C were predicted for 2070–2099, respectively. In the same fashion, ref. [62] stated that the increasing trend of precipitation was 6.1–17.7%, and the maximum temperature was 1.1–3.8 °C under different scenarios over the Upper Blue Nile Basin. Other findings in the wet season in the basin support the obtained result, but the resulting values are insignificantly different [140]. Furthermore, ref. [141] used GCMs CMIP5/6 to simulate precipitation and temperature over East Africa, and the GFDL-CM4 and NorESM2-MM models were selected as the best performing under near-future scenario SSP5852021-2050. The study results show a highly increasing trend of temperature, especially in lowland countries and some parts of Ethiopia's lower land. Decreasing and increasing trends of precipitation were also observed in the region.

Generally, the study findings show an increasing trend in precipitation and an increasing trend of maximum temperature, which agrees with the above-mentioned paper's result. It is impossible to generalize from any of this research because they all used various time scales, numbers, input data, climate model types, emission scenarios, and downscaling techniques, that all lead to inconsistent findings. In East Africa, particularly in Ethiopia, there is a significant degree of climate variation because of the country's challenging topography and vast variety of climatic conditions that influence a wide range of vegetation landscapes, biodiversity, and human vocations [142]. Rainfall distribution throughout different portions of Africa during all seasons is primarily influenced by the interplay of mountains and water bodies with the tropical Indo-Pacific climate drivers, the classic El Nino Southern Oscillation [ENSO], and Indian Ocean [143]. Understanding the variation of the projected future of climate change under different scenarios is vital in water resource management and watershed management. There is an implication of increasing land degradation, flooding with increasing precipitation over the basin, and increasing temperature, which also brings high evaporation loss. Therefore, it is crucial to strengthen soil and water conservation techniques in order to reduce the negative effects of future climate change on the basin.

5. Conclusions

In this study, the performance evaluation of 20 GCMs CMIP6 models was appropriately carried out to replicate the characteristics of precipitation and maximum temperature in the Omo River Basin. Their performance was assessed against the best-selected mean monthly CHIRPS precipitation and ERA5 maximum temperature values using mainly five statistical metric indicators such as NRMSE, Pbias, NSE, correlation coefficient (CC), and skill score (SS) for the baseline period of 1985–2014. Moreover, Taylor diagrams and temporal-spatial distributions were used to assess each CMIP6 model's ability to reproduce temperature and precipitation. The GCMs were selected and ranked using a compromise programming multi-criteria decision-making approach. Based on the statistical metrics and the ideal value (Lp), the GFDL-CM4 model shows the best performance among 20 CMIP6 models. However, the top three models ensemble shows a relatively better performance than the GFDL-CM4M model and was selected for future precipitation replication over the basin, while MIROC6 and ACCESS-ESM1-5 reveal the worst performance. In the case of maximum temperature, NorESM2-MM shows the best performance compared to others, including the 20 GCMs ensemble and top three models' ensemble, while KIOST-ESM and KACE-1-0-G show less skill in reproducing future maximum temperatures in the basin. According to the selected CMIP6 models, the spatial variation in mean monthly precipitation and maximum temperature over the basin is relatively well captured compared to reference data. However, overestimation and underestimation has been detected in some regions of the basin, such as in other models.

The best-performing models for precipitation and maximum temperature were downscaled and bias-corrected using SD-GCM2.0 software to evaluate future climate change in the basin. Additionally, the nonparametric Mann-Kendall trend test in R studio was utilized for the trend analysis. The projection of mean annual seasonal precipitation of the top three best-performing models, including their ensemble, shows an increasing trend in the near-future SSP2452031-2060 and SSP5852031-2060 scenarios, and the far-future SSP5852071-2100 scenario in both rainfall seasons of JJAS and MAM, except in the far-future SSP24571-2100 scenario in the JJAS season. However, overall, the change detected is insignificant. The spatial distribution of projected mean monthly precipitation shows that the southern part of the region will receive less precipitation and the central and northern areas, especially the northwestern area, will receive more precipitation in all scenarios. The anticipated seasonal maximum temperature time series of NorESM2-MM demonstrates a significant increase in trend over the basin in both near- and far-future scenarios. In all scenarios, the spatial distribution demonstrates that the southern and northern tips of the basin experience higher maximum temperatures than the center and northeastern portions of the basin.

The selection of general circulation models (GCMs) with a high ability to reflect the past and future climate for a specific geographic location is a critical first step in determining how climate change will affect water, agriculture, energy, and other sectors. This study used the recently released CMIP6, which has updated emission, concentration, and land-use scenarios known as shared socioeconomic pathways (SSPs, and allows for improved assessment of the impact of climate change policy. Despite the study area's tremendous potential regarding water resources for hydropower, irrigation, and other investments, continued global warming has led to unanticipated changes in the climate system that are negatively harming the basin. The results of this study can be utilized to forecast both future hydrological change and the availability of water resources in the basin. Furthermore, decision-makers can use the anticipated effects of climate change to establish mitigation and adaptation plans for the basin's watershed management and sustainable development of water resources. The information from this outcome will be used in later research analyzing how climate change will affect the basin and other upcoming climate change studies.

Author Contributions: Conceptualization, T.A.F., T.A.D., F.S. and A.G.; methodology, T.A.F.; software, T.A.F.; validation, T.A.F., T.A.D., F.S. and A.G.; formal analysis, T.A.F.; investigation, T.A.F.; resources, F.S. and A.G.; writing—original draft preparation, T.A.F.; writing—review and editing, T.A.F., T.A.D., F.S. and A.G.; supervision, T.A.D., F.S. and A.G. All authors have read and agreed to the published version of the manuscript.

Funding: This research received no external funding; however, the APC is funded by Rostock University via the University Library.

Institutional Review Board Statement: Not applicable.

Informed Consent Statement: Not applicable.

Data Availability Statement: The data used in this study can be available from the authors on reasonable request.

Acknowledgments: First of all, we would like to thank the Centre of Excellence in Science and Technology (EXiST) project, Jimma University, and the Jimma Institute of Technology for providing funds during study. Additionally, the authors thank Rostock University for providing resources and material support for the study, as well as their willingness to finance the publication under the funding program Open Access Publication.

Conflicts of Interest: The authors declare no conflict of interest.

Appendix A

Table A1. The result of Statistical indicators used in bias correction of the models corresponding to methods.

Precipitation Models	QDM (RMSE)	EQM (RMSE)	QM (RMSE)	QDM (CC)	EQM (CC)	QM (CC)	QDM (NSE)	EQM (NSE)	QM (NSE)
FGDL-CM4	**2.869**	3.909	3.936	0.497	**0.511**	0.508	**−0.153**	−1.149	−1.159
NorESM2-MM	**2.851**	3.947	3.848	**0.506**	0.493	0.508	**−0.184**	−1.063	−0.972
CanESM5	**2.956**	4.485	4.690	0.452	**0.490**	0.474	**−0.183**	−1.769	−2.080
Max. Temperature									
NorESM2-MM	**2.042**	2.059	2.103	0.649	**0.653**	0.649	0.295	**0.307**	0.276
MPI-ESM1-2-LR	2.187	**2.120**	2.157	0.638	**0.642**	0.638	0.187	**0.273**	0.247
CMCC-ESM2	2.186	**2.062**	2.230	0.642	**0.648**	0.639	0.183	**0.306**	0.184

The bold numbers indicates that the best values of statistical indicators corresponding to the methods.

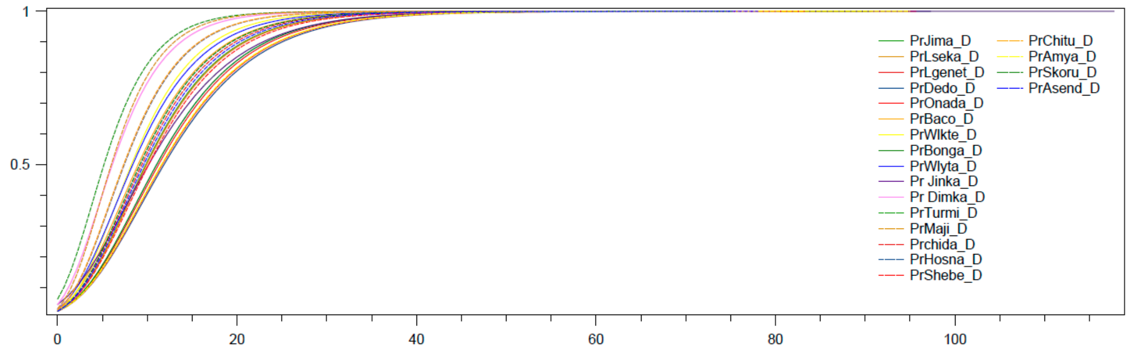

GFDL-CM4SSP2452031-2060

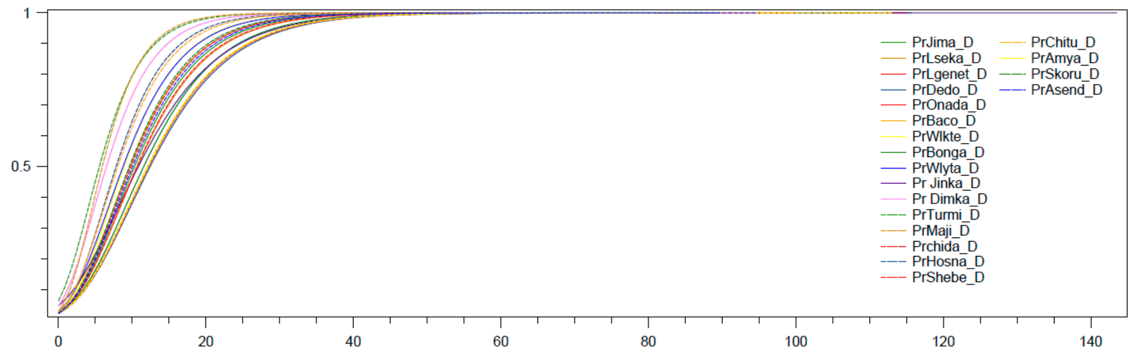

GFDL-CMSSP42452071-2100

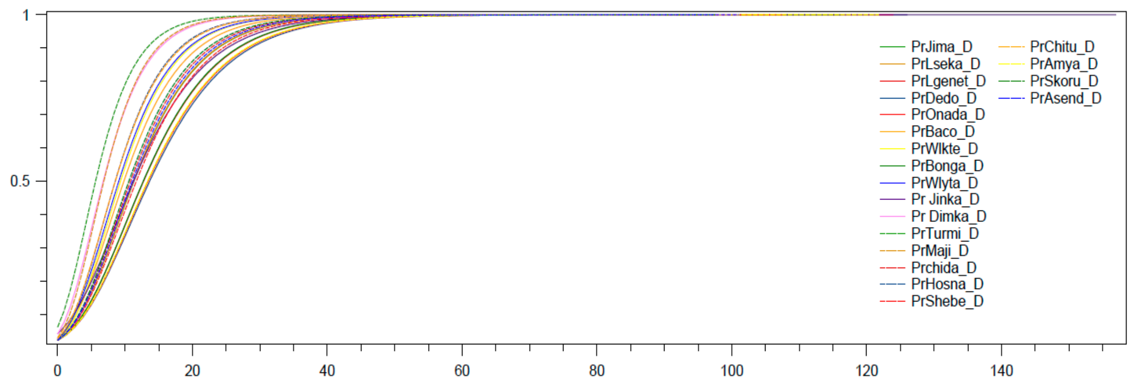

GFDL-CM4SSP5852031-2060

Figure A1. *Cont.*

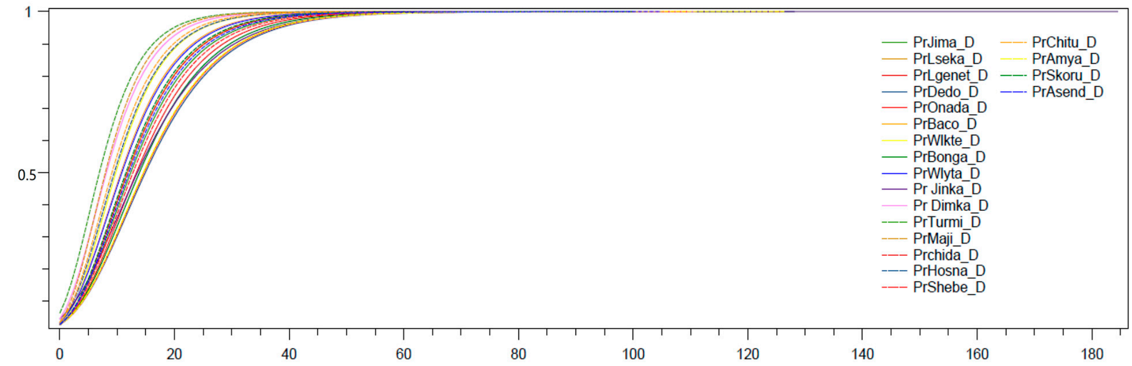

GFDL-CM4SSP5852071-2100

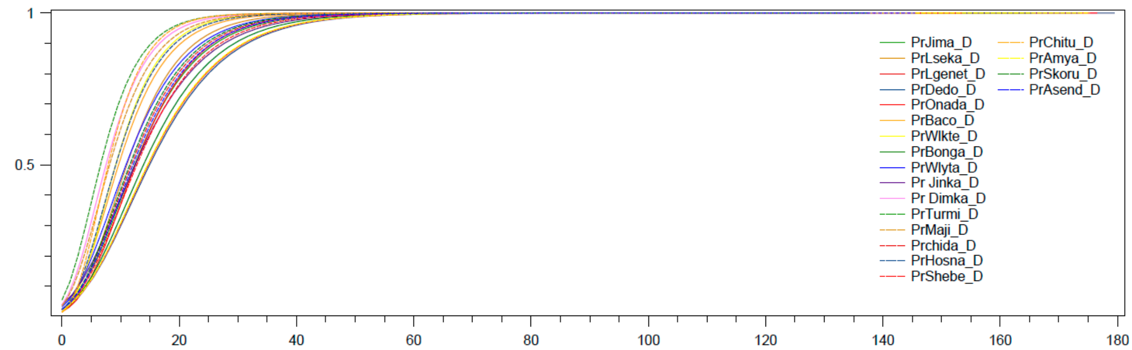

CanESM5SSP2452031-2060

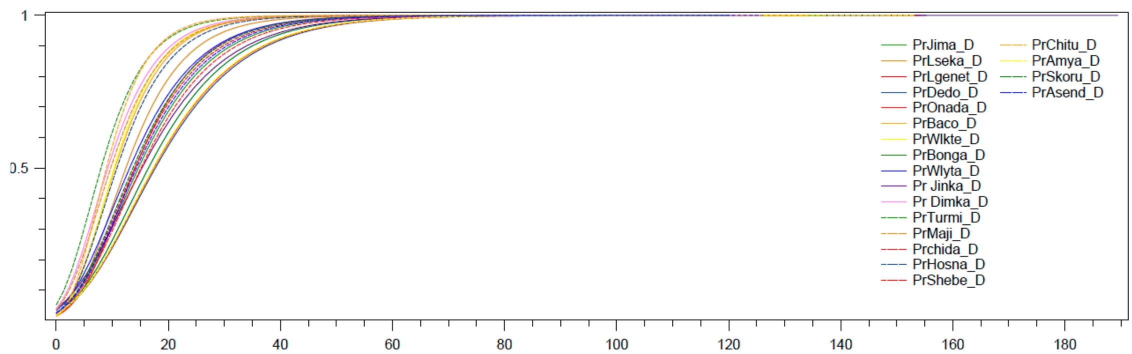

CanESM5SSP2452071-2100

Figure A1. *Cont*.

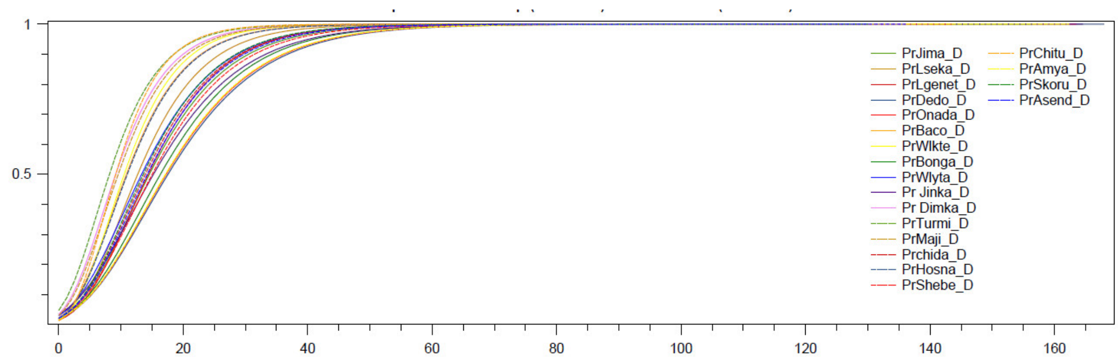

CanESM5SSP5852031-2060

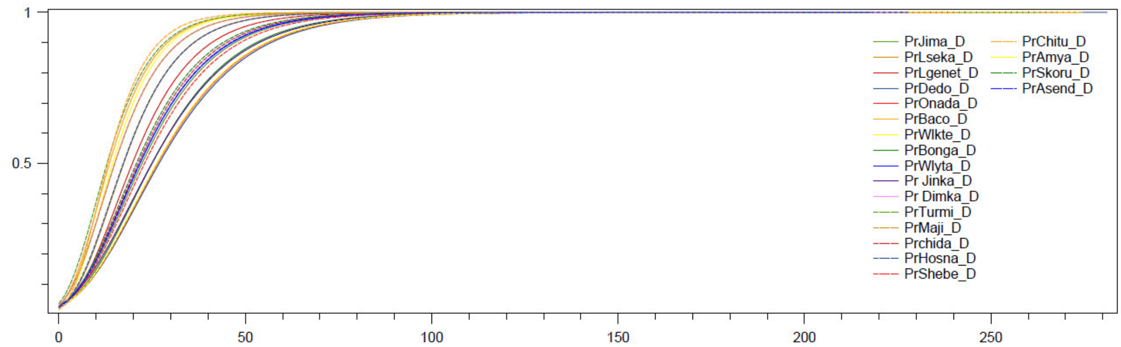

CanESM5SSP5852071-2100

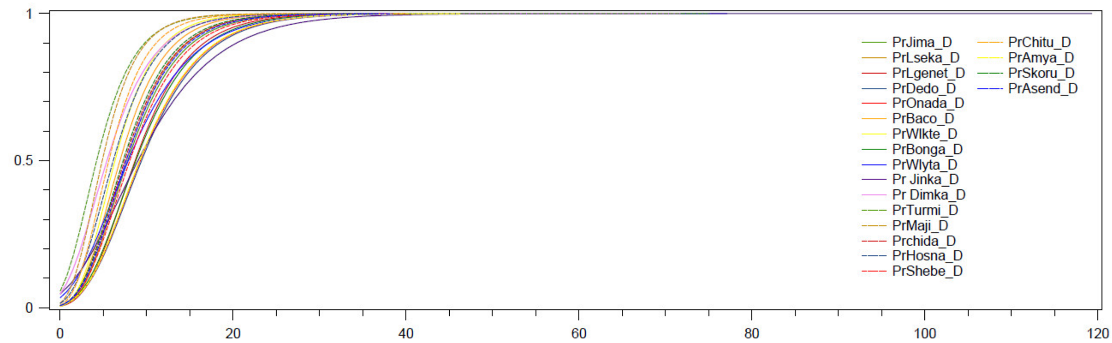

NorESM2-MMSSP2452031-2060

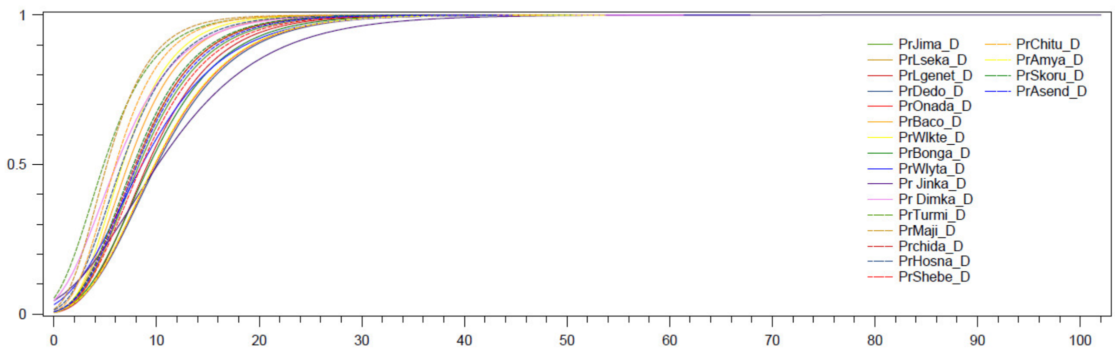

NorESM2-MMSSP2452071-2100

Figure A1. *Cont*.

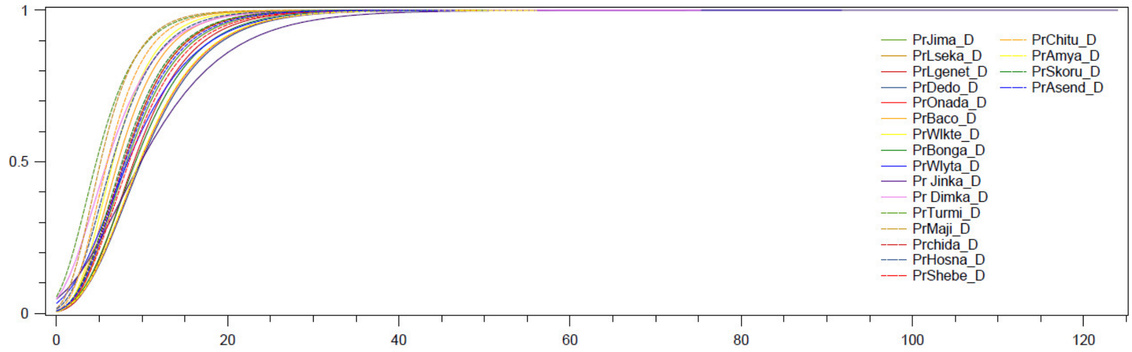

NorESM2-MMSSP5852031-2060

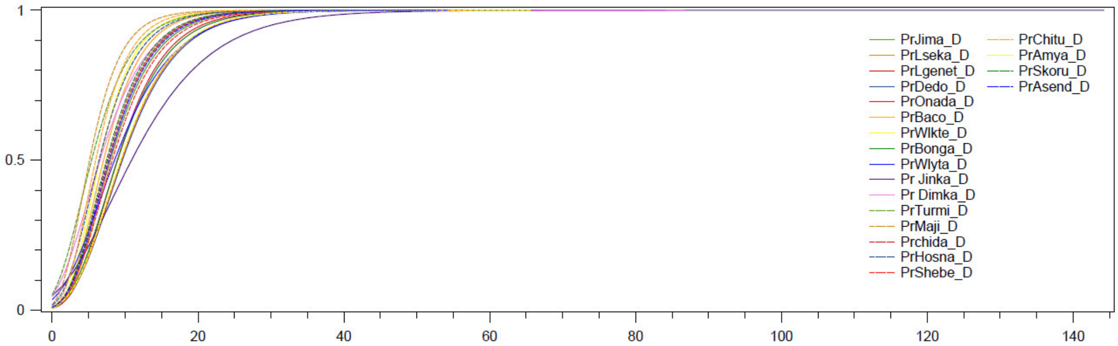

NorESM2-MMSSP5852071-2100

Figure A1. The cumulative distribution functions (CDF) of downscaled precipitation of GFDL-CM4, CanESM5 and NorESM2-MM models against observed under near (SSP245/5852031-2060) and far-future scenarios (SSP245/5852071-2100).

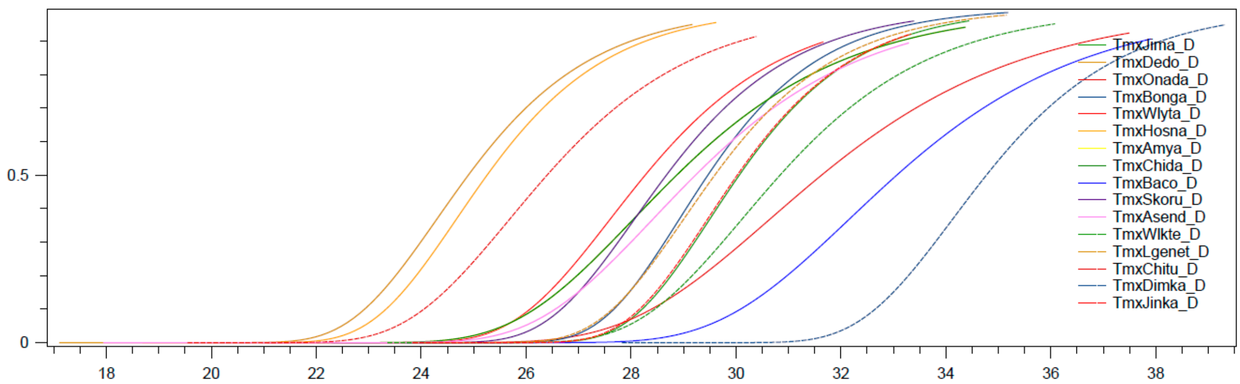

NorESM2-MMSSP2452031-2060

Figure A2. *Cont*.

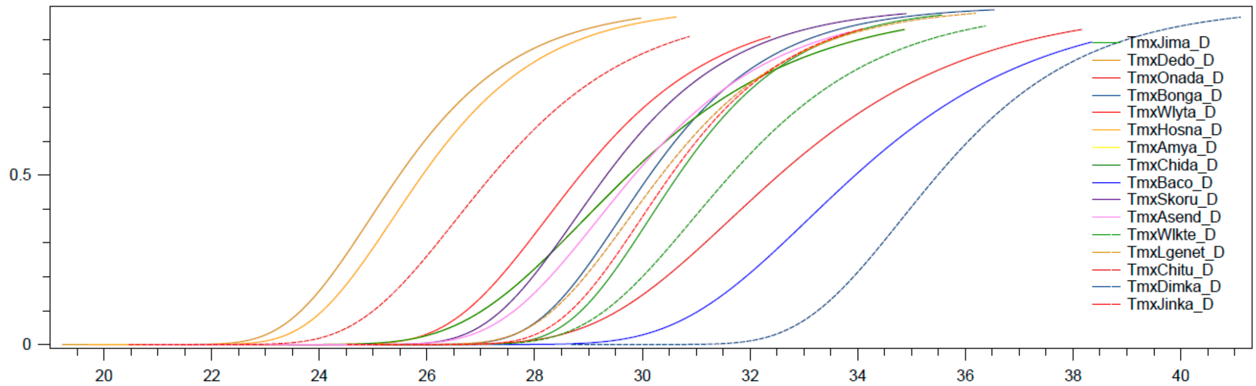

NorESM2-MMSSP2452071-2100

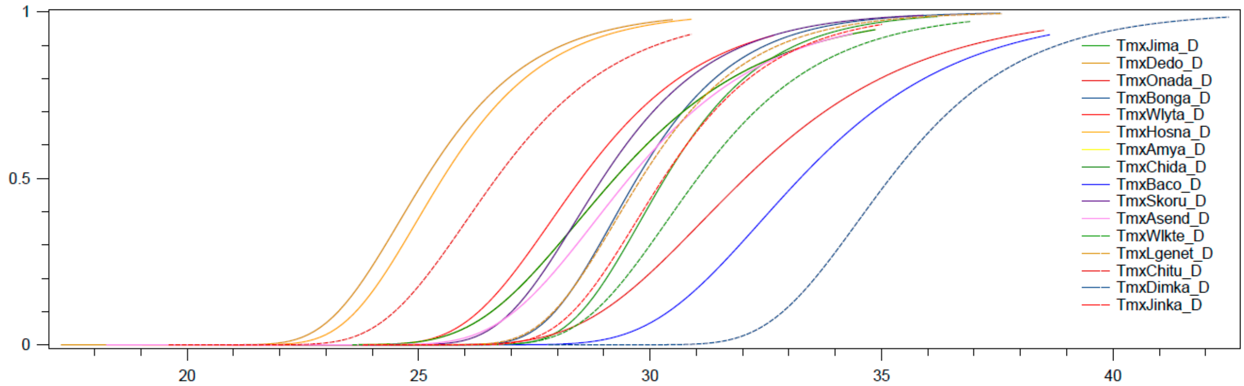

NorESM2-MMSSP5852031-2060

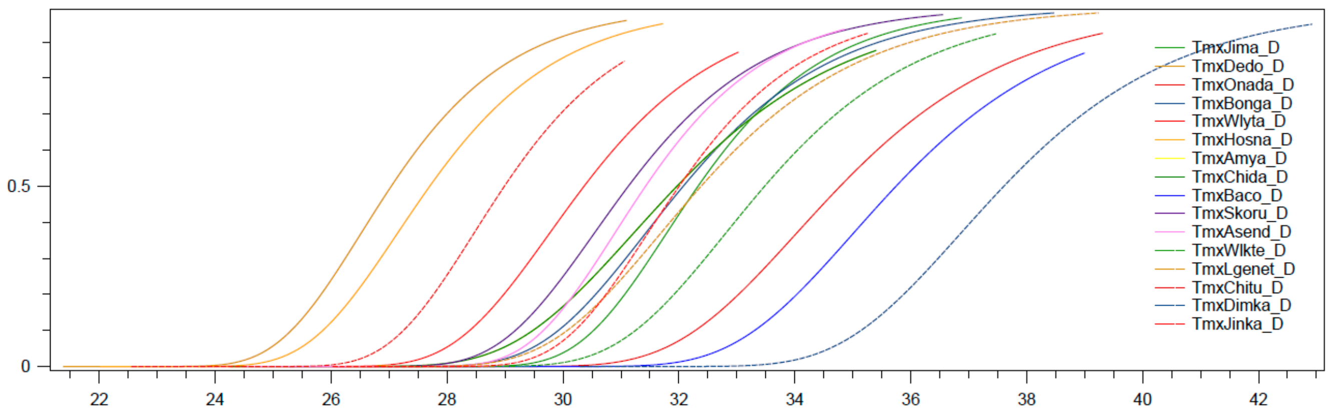

NorESM2-MMSSP5852071-2100

Figure A2. The cumulative distribution functions (CDF) of downscaled maximum temperature of NorESM2-MM against observed under near (SSP245/5852031-2060) and far-future scenarios (SSP245/5852071-2100).

References

1. Fenta Mekonnen, D.; Disse, M. Analyzing the Future Climate Change of Upper Blue Nile River Basin Using Statistical Downscaling Techniques. *Hydrol. Earth Syst. Sci.* **2018**, *22*, 2391–2408. [CrossRef]
2. Prof Critto, A. Climate Change: Impacts, Adaptation and Vulnerability. *Clim. Chang. Impacts Adapt. Vulnerability Approaches* **2009**, *8*, 419–429.

3. Ayugi, B.; Shilenje, Z.W.; Babaousmail, H.; Lim Kam Sian, K.T.C.; Mumo, R.; Dike, V.N.; Iyakaremye, V.; Chehbouni, A.; Ongoma, V. Projected Changes in Meteorological Drought over East Africa Inferred from Bias-Adjusted CMIP6 Models. *Nat. Hazards* **2022**, *113*, 1151–1176.
4. Singh, R.; Biswal, B. *Assessing the Impact of Climate Change on Water Resources: The Challenge Posed by a Multitude of Options*; Springer: Cham, Switzerland, 2019; pp. 185–204.
5. Wanders, N.; Wada, Y. Human and Climate Impacts on the 21st Century Hydrological Drought. *J. Hydrol.* **2015**, *526*, 208–220.
6. Caracciolo, D.; Pumo, D.; Arnone, E.; Francipane, A.; Caracciolo, D.; Noto, L.V. *Potential Implications of Climate Change and Urbanization on Watershed Hydrology*; Elsevier: Amsterdam, The Netherlands, 2017.
7. Ongoma, V.; Chen, H. Temporal and Spatial Variability of Temperature and Precipitation over East Africa from 1951 to 2010. *Meteorol. Atmos. Phys.* **2017**, *129*, 131–144.
8. Ayugi, B.; Zhihong, J.; Zhu, H.; Ngoma, H.; Babaousmail, H.; Rizwan, K.; Dike, V. Comparison of CMIP6 and CMIP5 Models in Simulating Mean and Extreme Precipitation over East Africa. *Int. J. Climatol.* **2021**, *41*, 6474–6496. [CrossRef]
9. Yengoh, G.T.; Ardö, J. Climate Change and the Future Heat Stress Challenges among Smallholder Farmers in East Africa. *Atmosphere* **2020**, *11*, 753. [CrossRef]
10. Cattani, E.; Merino, A.; Guijarro, J.A.; Levizzani, V. East Africa Rainfall Trends and Variability 1983–2015 Using Three Long-Term Satellite Products. *Remote Sens.* **2018**, *10*, 931. [CrossRef]
11. Ayugi, B.; Tan, G.; Gnitou, G.T.; Ojara, M.; Ongoma, V. Historical Evaluations and Simulations of Precipitation over East Africa from Rossby Centre Regional Climate Model. *Atmos. Res.* **2020**, *232*, 104705.
12. World Food Programme. *Status of Drought across the Eastern Horn*; World Food Programme: Rome, Italy, 2022.
13. Iyakaremye, V.; Zeng, G.; Yang, X.; Zhang, G.; Ullah, I.; Gahigi, A.; Vuguziga, F.; Asfaw, T.G.; Ayugi, B. Increased High-Temperature Extremes and Associated Population Exposure in Africa by the Mid-21st Century. *Sci. Total Environ.* **2021**, *790*, 148162. [CrossRef]
14. Ahmadalipour, A.; Moradkhani, H.; Castelletti, A.; Magliocca, N. Future Drought Risk in Africa: Integrating Vulnerability, Climate Change, and Population Growth. *Sci. Total Environ.* **2019**, *662*, 672–686. [PubMed]
15. Kassie, B.T.; Ittersum, V.M.; Rötter, R.; Hengsdijk, H.; Asseng, S. *Climate Variability and Change in Ethiopia: Exploring Impacts and Adaptation Options for Cereal Production*; Wageningen University: Wageningen, NL, USA, 2014.
16. Awulachew, S.; Yilma, A.; Loulseged, M.; Loiskandl, W. *Water Resources and Irrigation Development in Ethiopia*; IWMI: Colombo, Sri Lanka, 2007.
17. Anose, F.A.; Beketie, K.T.; Terefe Zeleke, T.; Yayeh Ayal, D.; Legese Feyisa, G. Spatio-Temporal Hydro-Climate Variability in Omo-Gibe River Basin, Ethiopia. *Clim. Serv.* **2021**, *24*, 100277.
18. Chaemiso, S.E.; Abebe, A.; Pingale, S.M. Assessment of the Impact of Climate Change on Surface Hydrological Processes Using SWAT: A Case Study of Omo-Gibe River Basin, Ethiopia. *Model. Earth Syst. Environ.* **2016**, *2*, 1–15. [CrossRef]
19. Bombelli, G.; Tomiet, S.; Bianchi, A.; Water, D.B. Impact of Prospective Climate Change Scenarios upon Hydropower Potential of Ethiopia in Gerd and Gibe Dams. *Water* **2021**, *13*, 716. [CrossRef]
20. Jaweso, D.; Abate, B.; Bauwe, A.; Lennartz, B. Hydro-Meteorological Trends in the Upper Omo-Ghibe River Basin, Ethiopia. *Water* **2019**, *11*, 1951. [CrossRef]
21. Orkodjo, T.P.; Kranjac-Berisavijevic, G.; Abagale, F.K. Impact of Climate Change on Future Precipitation Amounts, Seasonal Distribution, and Streamflow in the Omo-Gibe Basin, Ethiopia. *Heliyon* **2022**, *8*, e09711. [PubMed]
22. Babaousmail, H.; Hou, R.; Ayugi, B.; Ojara, M.; Ngoma, H.; Karim, R.; Rajasekar, A.; Ongoma, V. Evaluation of the Performance of Cmip6 Models in Reproducing Rainfall Patterns over North Africa. *Atmosphere* **2021**, *12*, 475. [CrossRef]
23. Baker, N.C.; Huang, H.P. A Comparative Study of Precipitation and Evaporation between CMIP3 and CMIP5 Climate Model Ensembles in Semiarid Regions. *J. Clim.* **2014**, *27*, 3731–3749. [CrossRef]
24. Eyring, V.; Bony, S.; Meehl, G.A.; Senior, C.A.; Stevens, B.; Stouffer, R.J.; Taylor, K.E. Overview of the Coupled Model Intercomparison Project Phase 6 (CMIP6) Experimental Design and Organization. *Geosci. Model Dev.* **2016**, *9*, 1937–1958.
25. Meehl, G.A.; Covey, C.; Delworth, T.; Latif, M.; McAvaney, B.; Mitchell, J.F.B.; Stouffer, R.J.; Taylor, K.E. The WCRP CMIP3 Multimodel Dataset: A New Era in Climatic Change Research. *Bull. Am. Meteorol. Soc.* **2007**, *88*, 1383–1394. [CrossRef]
26. Solomon, S.; Qin, D.; Manning, M.; Averyt, K.; Marquis, M. *Climate Change 2007—The Physical Science Basis: Working Group I Contribution to the Fourth Assessment Report of the IPCC*; Cambridge University Press: Cambridge, UK, 2007.
27. Taylor, K.E.; Stouffer, R.J.; Meehl, G.A. An Overview of CMIP5 and the Experiment Design. *Bull. Am. Meteorol. Soc.* **2012**, *93*, 485–498. [CrossRef]
28. Sperber, K.R.; Annamalai, H.; Kang, I.S.; Kitoh, A.; Moise, A.; Turner, A.; Wang, B.; Zhou, T. The Asian Summer Monsoon: An Intercomparison of CMIP5 vs. CMIP3 Simulations of the Late 20th Century. *Clim. Dyn.* **2013**, *41*, 2711–2744. [CrossRef]
29. Ogata, T.; Ueda, H.; Inoue, T.; Hayasaki, M.; Yoshida, A.; Watanabe, S.; Kira, M.; Ooshiro, M.; Kumai, A. Projected Future Changes in the Asian Monsoon: A Comparison of CMIP3 and CMIP5 Model Results. *J. Meteorol. Soc. Japan* **2014**, *92*, 207–225. [CrossRef]
30. Zhou, T.; Zou, L.; Chen, X. Commentary on the Coupled Model Intercomparison Project Phase 6 (CMIP6). *Clim. Chang. Res.* **2019**, *15*, 445–456.
31. Zhang, L.; Chen, X.; Xin, X. Short Commentary on CMIP6 Scenario Model Intercomparison Project (ScenarioMIP). *Clim. Chang. Res.* **2019**, *15*, 519–525.

32. Stouffer, R.J.; Eyring, V.; Meehl, G.A.; Bony, S.; Senior, C.; Stevens, B.; Taylor, K.E. CMIP5 Scientific Gaps and Recommendations for CMIP6. *Bull. Am. Meteorol. Soc.* **2017**, *98*, 95–105. [CrossRef]
33. Song, Y.H.; Chung, E.S.; Shahid, S. Spatiotemporal Differences and Uncertainties in Projections of Precipitation and Temperature in South Korea from CMIP6 and CMIP5 General Circulation Models. *Int. J. Climatol.* **2021**, *41*, 5899–5919. [CrossRef]
34. Iqbal, Z.; Shahid, S.; Ahmed, K.; Ismail, T.; Khan, N.; Virk, Z.T.; Johar, W. Evaluation of Global Climate Models for Precipitation Projection in Sub-Himalaya Region of Pakistan. *Atmos. Res.* **2020**, *245*, 105061. [CrossRef]
35. Salman, S.A.; Shahid, S.; Ismail, T.; Ahmed, K.; Wang, X.J. Selection of Climate Models for Projection of Spatiotemporal Changes in Temperature of Iraq with Uncertainties. *Atmos. Res.* **2018**, *213*, 509–522. [CrossRef]
36. Ahmed, K.; Sachindra, D.A.; Shahid, S.; Demirel, M.C.; Chung, E.S. Selection of Multi-Model Ensemble of General Circulation Models for the Simulation of Precipitation and Maximum and Minimum Temperature Based on Spatial Assessment Metrics. *Hydrol. Earth Syst. Sci.* **2019**, *23*, 4803–4824. [CrossRef]
37. Lin, C.Y.; Tung, C.P. Procedure for Selecting GCM Datasets for Climate Risk Assessment. *Terr. Atmos. Ocean. Sci.* **2017**, *28*, 43–55. [CrossRef]
38. Khan, A.J.; Koch, M. Selecting and Downscaling a Set of Climate Models for Projecting Climatic Change for Impact Assessment in the Upper Indus Basin (UIB). *Climate* **2018**, *6*, 89. [CrossRef]
39. Demirel, M.C.; Mai, J.; Mendiguren, G.; Koch, J.; Samaniego, L.; Stisen, S. Combining Satellite Data and Appropriate Objective Functions for Improved Spatial Pattern Performance of a Distributed Hydrologic Model. *Hydrol. Earth Syst. Sci.* **2018**, *22*, 1299–1315. [CrossRef]
40. Homsi, R.; Shiru, M.S.; Shahid, S.; Ismail, T.; Harun, S.B.; Al-Ansari, N.; Chau, K.W.; Yaseen, Z.M. Precipitation Projection Using a CMIP5 GCM Ensemble Model: A Regional Investigation of Syria. *Eng. Appl. Comput. Fluid Mech.* **2020**, *14*, 90–106. [CrossRef]
41. Lutz, A.F.; ter Maat, H.W.; Biemans, H.; Shrestha, A.B.; Wester, P.; Immerzeel, W.W. Selecting Representative Climate Models for Climate Change Impact Studies: An Advanced Envelope-Based Selection Approach. *Int. J. Climatol.* **2016**, *36*, 3988–4005. [CrossRef]
42. Shiru, M.S.; Shahid, S.; Chung, E.S.; Alias, N.; Scherer, L. A MCDM-Based Framework for Selection of General Circulation Models and Projection of Spatio-Temporal Rainfall Changes: A Case Study of Nigeria. *Atmos. Res.* **2019**, *225*, 1–16. [CrossRef]
43. Knutti, R.; Furrer, R.; Tebaldi, C.; Cermak, J.; Meehl, G.A. Challenges in Combining Projections from Multiple Climate Models. *J. Clim.* **2010**, *23*, 2739–2758. [CrossRef]
44. Shiru, M.S.; Chung, E.S. Performance Evaluation of CMIP6 Global Climate Models for Selecting Models for Climate Projection over Nigeria. *Theor. Appl. Climatol.* **2021**, *146*, 599–615. [CrossRef]
45. Rivera, J.A.; Arnould, G. Evaluation of the Ability of CMIP6 Models to Simulate Precipitation over Southwestern South America: Climatic Features and Long-Term Trends (1901–2014). *Atmos. Res.* **2020**, *241*, 104953. [CrossRef]
46. Sreelatha, K.; Anand Raj, P. Ranking of CMIP5-Based Global Climate Models Using Standard Performance Metrics for Telangana Region in the Southern Part of India. *ISH J. Hydraul. Eng.* **2021**, *27*, 556–565. [CrossRef]
47. Dibaba, W.T.; Miegel, K.; Demissie, T.A. Evaluation of the CORDEX Regional Climate Models Performance in Simulating Climate Conditions of Two Catchments in Upper Blue Nile Basin. *Dyn. Atmos. Ocean.* **2019**, *87*, 101104. [CrossRef]
48. Demissie, T.A.; Sime, C.H. Assessment of the performance of CORDEX regional climate models in simulating rainfall and air temperature over southwest Ethiopia. *Heliyon* **2021**, *7*, e07791. [CrossRef]
49. Ayugi, B.; Ngoma, H.; Babaousmail, H.; Karim, R.; Iyakaremye, V.; Lim Kam Sian, K.T.C.; Ongoma, V. Evaluation and Projection of Mean Surface Temperature Using CMIP6 Models over East Africa. *J. African Earth Sci.* **2021**, *181*, 104226. [CrossRef]
50. Klutse, N.A.B.; Quagraine, K.A.; Nkrumah, F.; Quagraine, K.T.; Berkoh-Oforiwaa, R.; Dzrobi, J.F.; Sylla, M.B. The Climatic Analysis of Summer Monsoon Extreme Precipitation Events over West Africa in CMIP6 Simulations. *Earth Syst. Environ.* **2021**, *5*, 25–41. [CrossRef]
51. Hajkowicz, S.; Collins, K. A Review of Multiple Criteria Analysis for Water Resource Planning and Management. *Water Resour. Manag.* **2007**, *21*, 1553–1566. [CrossRef]
52. Houngue, N.R.; Delos, A.; Almoradie, S.; Evers, M. A Multi Criteria Decision Analysis Approach for Regional Climate Model Selection and Future Climate Assessment in the Mono River Basin, Benin and Togo. *Atmosphere* **2022**, *13*, 1471. [CrossRef]
53. Salehie, O.; Hamed, M.; Ismail, T.; Tam, T.; Shahid, S. Selection of CMIP6 GCM With Projection of Climate over The Amu Darya River Basin. *Prepr. Available Res. Sq.* **2021**, *151*, 1–27. [CrossRef]
54. Srinivasa Raju, K.; Sonali, P.; Nagesh Kumar, D. Ranking of CMIP5-Based Global Climate Models for India Using Compromise Programming. *Theor. Appl. Climatol.* **2017**, *128*, 563–574. [CrossRef]
55. Raju, K.S.; Kumar, D.N. Ranking of Global Climate Models for India Using Multicriterion Analysis. *Clim. Res.* **2014**, *60*, 103–117. [CrossRef]
56. Meaurio, M.; Zabaleta, A.; Boithias, L.; Epelde, A.M.; Sauvage, S.; Sánchez-Pérez, J.M.; Srinivasan, R.; Antiguedad, I. Assessing the Hydrological Response from an Ensemble of CMIP5 Climate Projections in the Transition Zone of the Atlantic Region (Bay of Biscay). *J. Hydrol.* **2017**, *548*, 46–62. [CrossRef]
57. Ringuest, J.L. Compromise Programming. In *Multiobjective Optimization: Behavioral and Computational Considerations*; Springer: Boston, MA, USA, 1992; pp. 51–59.

58. Kaini, S.; Santosh Nepal, I.; Saurav Pradhananga, I.; Gardner, T.; Sharma, A.K. Representative General Circulation Models Selection and Downscaling of Climate Data for the Transboundary Koshi River Basin in China and Nepal. *Wiley Online Libr.* **2019**, *40*, 4131–4149. [CrossRef]
59. Liu, F.; Xu, C.; Long, Y.; Yin, G.; Wang, H. Assessment of CMIP6 Model Performance for Air Temperature in the Arid Region of Northwest China and Subregions. *Atmosphere* **2022**, *13*, 454. [CrossRef]
60. Mbigi, D.; Onyango, A.; Mtewele, Z.F.; Kiprotich, P.; Xiao, Z. CMIP6 Simulations of the Spatial Structure of Rainfall Variability over East Africa: Evaluation and Projection. *Int. J. Climatol.* **2022**, *42*, 9865–9885. [CrossRef]
61. Gebresellase, S.H.; Wu, Z.; Xu, H.; Muhammad, W.I. Evaluation and Selection of CMIP6 Climate Models in Upper Awash Basin (UBA), Ethiopia. *Theor. Appl. Climatol.* **2022**, *149*, 1521–1547. [CrossRef]
62. Alaminie, A.A.; Tilahun, S.A.; Legesse, S.A.; Zimale, F.A.; Tarkegn, G.B.; Jury, M.R.; Theodoros, M. Evaluation of Past and Future Climate Trends under CMIP6 Scenarios for the UBNB (Abay), Ethiopia. *Water* **2021**, *13*, 2110. [CrossRef]
63. Degefu, M.A.; Bewket, W. Variability and Trends in Rainfall Amount and Extreme Event Indices in the Omo-Ghibe River Basin, Ethiopia. *Reg. Environ. Chang.* **2014**, *14*, 799–810. [CrossRef]
64. Worku, F.F.; Werner, M.; Wright, N.; Van Der Zaag, P.; Demissie, S.S. Flow Regime Change in an Endorheic Basin in Southern Ethiopia. *Hydrol. Earth Syst. Sci.* **2014**, *18*, 3837–3853. [CrossRef]
65. Namara, W.G.; Hirpo, G.M.; Feyissa, T.A. Evaluation of Impact of Climate Change on the Watershed Hydrology, Case of Wabe Watershed, Omo Gibe River Basin, Ethiopia. *Arab. J. Geosci.* **2022**, *15*, 1–15. [CrossRef]
66. Stern, R.; Rijks, D.; Dale, I.; Knock, J. *INSTAT Climatic Guide*; University of Reading: Reading, UK, 2006; pp. 247–281.
67. Dinku, T. Challenges with Availability and Quality of Climate Data in Africa. In *Extreme Hydrology and Climate Variability*; Elsevier: Amsterdam, The Netherlands, 2019; pp. 71–80.
68. Dinku, T.; Faniriantsoa, R.; Islam, S.; Nsengiyumva, G.; Grossi, A. The Climate Data Tool: Enhancing Climate Services Across Africa. *Front. Clim.* **2022**, *3*, 185. [CrossRef]
69. Wilby, R.; Yu, D. Rainfall and Temperature Estimation for a Data Sparse Region. *Hydrol. Earth Syst. Sci.* **2013**, *17*, 3937–3955. [CrossRef]
70. Dinku, T.; Hailemariam, K.; Maidment, R.; Tarnavsky, E.; Connor, S. Combined Use of Satellite Estimates and Rain Gauge Observations to Generate High-Quality Historical Rainfall Time Series over Ethiopia. *Int. J. Climatol.* **2014**, *34*, 2489–2504. [CrossRef]
71. Nikulin, G.; Jones, C.; Giorgi, F.; Asrar, G.; Büchner, M.; Cerezo-Mota, R.; Christensen, O.B.; Déqué, M.; Fernandez, J.; Hänsler, A.; et al. Precipitation Climatology in an Ensemble of CORDEX-Africa Regional Climate Simulations. *J. Clim.* **2012**, *25*, 6057–6078. [CrossRef]
72. Sylla, M.B.; Giorgi, F.; Coppola, E.; Mariotti, L. Uncertainties in Daily Rainfall over Africa: Assessment of Gridded Observation Products and Evaluation of a Regional Climate Model Simulation. *Int. J. Climatol.* **2013**, *33*, 1805–1817. [CrossRef]
73. Funk, C.; Peterson, P.; Landsfeld, M.; Davenport, F.; Becker, A.; Schneider, U.; Pedreros, D.; McNally, A.; Arsenault, K.; Harrison, L.; et al. Algorithm and Data Improvements for Version 2.1 of the Climate Hazards Center's InfraRed Precipitation with Stations Data Set. *Adv. Glob. Chang. Res.* **2020**, *67*, 409–427.
74. Harris, I.; Osborn, T.J.; Jones, P.; Lister, D. Version 4 of the CRU TS Monthly High-Resolution Gridded Multivariate Climate Dataset. *Sci. Data* **2020**, *7*, 1–18. [CrossRef]
75. Xie, P.; Yatagai, A.; Chen, M.; Hayasaka, T.; Fukushima, Y.; Liu, C.; Yang, S. A Gauge-Based Analysis of Daily Precipitation over East Asia. *J. Hydrometeorol.* **2007**, *8*, 607–626. [CrossRef]
76. Ehsani, M.; Behrangi, A. On the Importance of Gauge-Undercatch Correction Factors and Their Impacts on the Global Precipitation Estimates. *Preprint* **2021**, 202106.0179.
77. Hersbach, H.; Bell, B.; Berrisford, P.; Hirahara, S.; Horányi, A.; Muñoz-Sabater, J.; Nicolas, J.; Peubey, C.; Radu, R.; Schepers, D.; et al. The ERA5 Global Reanalysis. *Q. J. R. Meteorol. Soc.* **2020**, *146*, 1999–2049. [CrossRef]
78. Aha, S.S.; Adiga, S.N.; Hiaw, C.T.; Ang, J.W.; Saha, S.; Nadiga, S.; Thiaw, C.; Wang, J.; Wang, W.; Zhang, Q.; et al. The NCEP Climate Forecast System. *J. Clim.* **2006**, *19*, 3483–3517.
79. O'Neill, B.C.; Kriegler, E.; Ebi, K.L.; Kemp-Benedict, E.; Riahi, K.; Rothman, D.S.; van Ruijven, B.J.; van Vuuren, D.P.; Birkmann, J.; Kok, K.; et al. The Roads Ahead: Narratives for Shared Socioeconomic Pathways Describing World Futures in the 21st Century. *Glob. Environ. Chang.* **2017**, *42*, 169–180. [CrossRef]
80. O'neill, B.C.; Tebaldi, C.; Van Vuuren, D.P.; Eyring, V.; Friedlingstein, P.; Hurtt, G.; Knutti, R.; Kriegler, E.; Lamarque, J.-F.; Lowe, J.; et al. The Scenario Model Intercomparison Project (ScenarioMIP) for CMIP6. *Geosci. Model Dev.* **2016**, *9*, 3461–3482. [CrossRef]
81. Gidden, M.J.; Riahi, K.; Smith, S.J.; Fujimori, S.; Luderer, G.; Kriegler, E.; Van Vuuren, D.P.; Van Den Berg, M.; Feng, L.; Klein, D.; et al. Global Emissions Pathways under Different Socioeconomic Scenarios for Use in CMIP6: A Dataset of Harmonized Emissions Trajectories through the End of the Century. *Geosci. Model Dev.* **2019**, *12*, 1443–1475. [CrossRef]
82. Bi, D.; Dix, M.; Marsland, S.; O'farrell, S.; Sullivan, A.; Bodman, R.; Law, R.; Harman, I.; Srbinovsky, J.; Rashid, H.A.; et al. Configuration and Spin-up of ACCESS-CM2, the New Generation Australian Community Climate and Earth System Simulator Coupled Model. *J. South. Hemisph. Earth Syst. Sci.* **2020**, *70*, 225–251. [CrossRef]
83. Ziehn, T.; Chamberlain, M.A.; Law, R.M.; Lenton, A.; Bodman, R.W.; Dix, M.; Stevens, L.; Wang, Y.P.; Srbinovsky, J. The Australian Earth System Model: ACCESS-ESM1.5. *J. South. Hemisph. Earth Syst. Sci.* **2020**, *70*, 193–214. [CrossRef]

84. Wu, T.; Yu, R.; Lu, Y.; Jie, W.; Fang, Y.; Zhang, J.; Zhang, L.; Xin, X.; Li, L.; Wang, Z. BCC-CSM2-HR: A High-Resolution Version of the Beijing Climate Center Climate System Model. *Geosci. Model Dev.* **2021**, *14*, 2977–3006. [CrossRef]
85. Swart, N.; Scinocca, J.; Arora, V.; Christian, J.; Cole, J. The Canadian Earth System Model Version 5 Stable of Models at CCCma. *Geosci. Model Dev.* **2019**, *12*, 4823–4873. [CrossRef]
86. Cherchi, A.; Fogli, P.G.; Lovato, T.; Peano, D.; Iovino, D.; Gualdi, S.; Masina, S.; Scoccimarro, E.; Materia, S.; Bellucci, A.; et al. Global Mean Climate and Main Patterns of Variability in the CMCC-CM2 Coupled Model. *Wiley Online Libr.* **2019**, *11*, 185–209. [CrossRef]
87. Held, I.M.; Guo, H.; Adcroft, A.; Dunne, J.P.; Horowitz, L.W.; Krasting, J.; Shevliakova, E.; Winton, M.; Zhao, M.; Bushuk, M.; et al. Structure and Performance of GFDL's CM4.0 Climate Model. *J. Adv. Model. Earth Syst.* **2019**, *11*, 3691–3727. [CrossRef]
88. Dunne, J.P.; Horowitz, L.W.; Adcroft, A.J.; Ginoux, P.; Held, I.M.; John, J.G.; Krasting, J.P.; Malyshev, S.; Naik, V.; Paulot, F.; et al. The GFDL Earth System Model Version 4.1 (GFDL-ESM 4.1): Overall Coupled Model Description and Simulation Characteristics. *J. Adv. Model. Earth Syst.* **2020**, *12*, e2019MS002015. [CrossRef]
89. Volodin, E.M.; Mortikov, E.V.; Kostrykin, S.V.; Galin, V.Y.; Lykossov, V.N.; Gritsun, A.S.; Diansky, N.A.; Gusev, A.V.; Iakovlev, N.G.; Shestakova, A.A.; et al. Simulation of the Modern Climate Using the INM-CM48 Climate Model. *Russ. J. Numer. Anal. Math. Model.* **2018**, *33*, 367–374. [CrossRef]
90. Boucher, O.; Servonnat, J.; Albright, A.L.; Aumont, O.; Balkanski, Y.; Bastrikov, V.; Bekki, S.; Bonnet, R.; Bony, S.; Bopp, L.; et al. Presentation and Evaluation of the IPSL-CM6A-LR Climate Model. *J. Adv. Model. Earth Syst.* **2020**, *12*, e2019MS002010. [CrossRef]
91. Lee, J.; Kim, J.; Sun, M.A.; Kim, B.H.; Moon, H.; Sung, H.M.; Kim, J.; Byun, Y.H. Evaluation of the Korea Meteorological Administration Advanced Community Earth-System Model (K-ACE). *Asia-Pacific J. Atmos. Sci.* **2020**, *56*, 381–395. [CrossRef]
92. Pak, G.; Noh, Y.; Lee, M.I.; Yeh, S.W.; Kim, D.; Kim, S.Y.; Lee, J.L.; Lee, H.J.; Hyun, S.H.; Lee, K.Y.; et al. Korea Institute of Ocean Science and Technology Earth System Model and Its Simulation Characteristics. *Ocean Sci. J.* **2021**, *56*, 18–45. [CrossRef]
93. Tatebe, H.; Ogura, T.; Nitta, T.; Komuro, Y.; Ogochi, K.; Takemura, T.; Sudo, K.; Sekiguchi, M.; Abe, M.; Saito, F.; et al. Description and Basic Evaluation of Simulated Mean State, Internal Variability, and Climate Sensitivity in MIROC6. *Geosci. Model Dev.* **2019**, *12*, 2727–2765. [CrossRef]
94. Gutjahr, O.; Putrasahan, D.; Lohmann, K.; Jungclaus, J.H.; Von Storch, J.S.; Brüggemann, N.; Haak, H.; Stössel, A. Max Planck Institute Earth System Model (MPI-ESM1.2) for the High-Resolution Model Intercomparison Project (HighResMIP). *Geosci. Model Dev.* **2019**, *12*, 3241–3281.
95. Mauritsen, T.; Bader, J.; Becker, T.; Behrens, J.; Bittner, M.; Brokopf, R. Developments in the MPI-M Earth System Model Version 1.2 (MPI-ESM1.2) and Its Response to Increasing CO2. *Wiley Online Libr.* **2019**, *11*, 11.
96. Yukimoto, S.; Kawai, H.; Koshiro, T.; Oshima, N.; Yoshida, K.; Urakawa, S.; Tsujino, H.; Deushi, M.; Tanaka, T.; Hosaka, M.; et al. The Meteorological Research Institute Earth System Model Version 2.0, MRI-ESM2.0: Description and Basic Evaluation of the Physical Component. *J. Meteorol. Soc. Japan* **2019**, *97*, 931–965. [CrossRef]
97. Cao, J.; Wang, B.; Yang, Y.M.; Ma, L.; Li, J.; Sun, B.; Bao, Y.; He, J.; Zhou, X.; Wu, L. The NUIST Earth System Model (NESM) Version 3: Description and Preliminary Evaluation. *Geosci. Model Dev.* **2018**, *11*, 2975–2993. [CrossRef]
98. Seland, Ø.; Bentsen, M.; Olivié, D.; Toniazzo, T.; Gjermundsen, A.; Graff, L.S.; Debernard, B.; Gupta, A.K.; He, Y.; Kirkevåg, A.; et al. Overview of the Norwegian Earth System Model (NorESM2) and Key Climate Response of CMIP6 DECK, Historical, and Scenario Simulations. *Geosci. Model Dev.* **2020**, *13*, 6165–6200. [CrossRef]
99. Wang, Y.C.; Hsu, H.H.; Chen, C.A.; Tseng, W.L.; Hsu, P.C.; Lin, C.W.; Chen, Y.L.; Jiang, L.C.; Lee, Y.C.; Liang, H.C.; et al. Performance of the Taiwan Earth System Model in Simulating Climate Variability Compared with Observations and CMIP6 Model Simulations. *J. Adv. Model. Earth Syst.* **2021**, *13*, e2020MS002353. [CrossRef]
100. Yimer, S.M.; Bouanani, A.; Kumar, N.; Tischbein, B.; Borgemeister, C. Assessment of Climate Models Performance and Associated Uncertainties in Rainfall Projection from CORDEX over the Eastern Nile Basin, Ethiopia. *Climate* **2022**, *10*, 95. [CrossRef]
101. Rathinasamy, M.; Khosa, R.; Adamowski, J.; Ch, S.; Partheepan, G.; Anand, J.; Narsimlu, B. Wavelet-Based Multiscale Performance Analysis: An Approach to Assess and Improve Hydrological Models. *Water Resour. Res.* **2014**, *50*, 9721–9737. [CrossRef]
102. Srinivasa Raju, K.; Nagesh Kumar, D. Invited Review Paper Review of Approaches for Selection and Ensembling of GCMs. *J. Water Clim. Change* **2020**, *11*, 577–599. [CrossRef]
103. Nash, J.E.; Sutcliffe, J. V River Flow Forecasting Through Conceptual Models—Part I—A Discussion of Principles. *J. Hydrol.* **1970**, *10*, 282–290. [CrossRef]
104. Moriasi, D.N.; Arnold, J.G.; van Liew, M.W.; Bingner, R.L.; Harmel, R.D.; Veith, T.L. Model Evaluation Guidelines for Systematic Quantification of Accuracy in Watershed Simulations. *Trans. ASABE* **2007**, *50*, 885–900. [CrossRef]
105. Chen, F.W.; Liu, C.W. Estimation of the Spatial Rainfall Distribution Using Inverse Distance Weighting (IDW) in the Middle of Taiwan. *Paddy Water Environ.* **2012**, *10*, 209–222. [CrossRef]
106. Willmott, C.J. Some Comments on the Evaluation of Model Performance. *Bull.-Am. Meteorol. Soc.* **1982**, *63*, 1309–1313. [CrossRef]
107. Legates, D.R.; McCabe, G.J. Evaluating the Use of 'goodness-of-Fit' Measures in Hydrologic and Hydroclimatic Model Validation. *Water Resour. Res.* **1999**, *35*, 233–241. [CrossRef]
108. Raju, K.; Srinivasa, D.N.K. Impact of Climate Change on Water Resources. *Clim. Chang. Model. Plan. Policy Agric.* **2018**, 219–231.
109. Taylor, K.E. Summarizing Multiple Aspects of Model Performance in a Single Diagram. *J. Geophys. Res. Atmos.* **2001**, *106*, 7183–7192. [CrossRef]

110. Luo, N.; Guo, Y.; Chou, J.; Gao, Z. Added Value of CMIP6 Models over CMIP5 Models in Simulating the Climatological Precipitation Extremes in China. *Int. J. Climatol.* **2021**, *42*, 1148–1164. [CrossRef]
111. Mcmahon, S.; Peterson, N.A.; Winter, S.C.; Palmer, J.E.; Postmus, J.L.; Ruth, A.K. Predicting Bystander Behavior to Prevent Sexual Assault on College Campuses: The Role of Self-Efficacy and Intent. *Am. J. Community Psychol.* **2015**, *56*, 46–56. [CrossRef] [PubMed]
112. Zeleny, M. Compromise Programming. In *Multiple Criteria Decision Making*; Springer: Berlin/Heidelberg, Germany, 1973; pp. 51–59.
113. Ahmed, K.; Shahid, S.; Sachindra, D.A.; Nawaz, N.; Chung, E.S. Fidelity Assessment of General Circulation Model Simulated Precipitation and Temperature over Pakistan Using a Feature Selection Method. *J. Hydrol.* **2019**, *573*, 281–298. [CrossRef]
114. Bhadran, D.; Nair, S.; Mirajkar, A.; Deepthi, B.; Sunil, A.; Nair, S.C.; Mirajkar, A.B.; Adarsh, S. Ranking of CMIP5-Based General Circulation Models Using Compromise Programming and TOPSIS for Precipitation: A Case Study of Upper Godavari Basin, India. *World Sci.* **2020**, *2*, 2050007.
115. Pradhan, P.; Shrestha, S.; Sundaram, S.M.; Virdis, S.G.P. Evaluation of the CMIP5 General Circulation Models for Simulating the Precipitation and Temperature of the Koshi River Basin in Nepal. *J. Water Clim. Chang.* **2021**, *12*, 3282–3296. [CrossRef]
116. Pomerol, J.-C.; Barba-Romero, S. *Multicriterion Decision in Practice*; Springer: Berlin/Heidelberg, Germany, 2000; pp. 299–326.
117. Kiros, G.; Shetty, A.; Nandagiri, L. Analysis of Variability and Trends in Rainfall over Northern Ethiopia. *Arab. J. Geosci.* **2016**, *9*, 451. [CrossRef]
118. Koudahe, K.; Kayode, A.J.; Samson, A.O.; Adebola, A.A.; Djaman, K. Trend Analysis in Standardized Precipitation Index and Standardized Anomaly Index in the Context of Climate Change in Southern Togo. *Atmos. Clim. Sci.* **2017**, *07*, 401–423. [CrossRef]
119. Amin, A.; Nasim, W.; Mubeen, M.; Kazmi, H.; Lin, Z.; Wahid, A.; Refat Sultana, S.; Gibbs, J.; Fahad, S. *Comparison of Future and Base Precipitation Anomalies by SimCLIM Statistical Projection through Ensemble Approach in Pakistan*; Elsevier: Amsterdam, The Netherlands, 2017; Volume 194, pp. 214–225.
120. Ongoma, V.; Chen, H.; Omony, G.W. Variability of Extreme Weather Events over the Equatorial East Africa, a Case Study of Rainfall in Kenya and Uganda. *Theor. Appl. Climatol.* **2018**, *131*, 295–308. [CrossRef]
121. Salami, A.W.; Olanlokun, O.; Salami, A.W.; Mohammed, A.A.; Abdulmalik, Z.H.; Olanlokun, O.K. Trend Analysis of Hydro-Meteorological Variables Using the Mann-Kendall Trend Test: Application to the Niger River and the Benue Sub-Basins in Nigeria. *Int. J. Technol.* **2014**, *2*, 100–110. [CrossRef]
122. Tabari, H.; Somee, B.S.; Zadeh, M.R. Testing for Long-Term Trends in Climatic Variables in Iran. *Atmos. Res.* **2011**, *100*, 132–140. [CrossRef]
123. Sime, C.H.; Demissie, T.A. Assessment and Prediction of the Climate Change Impact on Crop Yield, in Jimma Zone Upper Gilgel Gibe Districts, Ethiopia. *Arab. J. Geosci.* **2022**, *15*, 1–15. [CrossRef]
124. Tebaldi, C.; Smith, R.L.; Nychka, D.; Mearns, L.O. Quantifying Uncertainty in Projections of Regional Climate Change: A Bayesian Approach to the Analysis of Multimodel Ensembles. *J. Clim.* **2005**, *18*, 1524–1540. [CrossRef]
125. Hamed, M.M.; Nashwan, M.S.; Shahid, S. Inter-Comparison of Historical Simulation and Future Projections of Rainfall and Temperature by CMIP5 and CMIP6 GCMs over Egypt. *Int. J. Climatol.* **2022**, *42*, 4316–4332. [CrossRef]
126. Salman, S.A.; Nashwan, M.S.; Ismail, T.; Shahid, S. Selection of CMIP5 General Circulation Model Outputs of Precipitation for Peninsular Malaysia. *Hydrol. Res.* **2020**, *51*, 781–798. [CrossRef]
127. Orkodjo, T.P.; Kranjac-Berisavijevic, G.; Abagale, F.K. Abagale. Impact of climate change on future availability of water for irrigation and hydropower generation in the Omo-Gibe Basin of Ethiopia. *J. Hydrol. Reg. Stud.* **2022**, *44*, 101254. [CrossRef]
128. Krakauer, N.Y.; Abebe Balcha, Y.; Malcherek, A.; Alamirew, T. Understanding Future Climate in the Upper Awash Basin (UASB) with Selected Climate Model Outputs under CMIP6. *Climate* **2022**, *10*, 185.
129. Zhu, H.; Jiang, Z.; Li, L. Projection of Climate Extremes in China, an Incremental Exercise from CMIP5 to CMIP6. *Sci. Bull.* **2021**, *66*, 2528–2537. [CrossRef] [PubMed]
130. Tewari, K.; Mishra, S.; Salunke, P.; Dewan, A. Future Projections of Temperature and Precipitation for Antarctica. *Environ. Res. Lett.* **2022**, *17*, 014029. [CrossRef]
131. Tong, M.; Zheng, Z.; Fu, Q. Evaluation of East Asian Meiyu from CMIP6/AMIP Simulations. *Clim. Dyn.* **2022**, *59*, 2429–2444. [CrossRef]
132. Nath Raila, S.; Acharya, R.; Ghimire, S.; Adhikari, S.; Khanal, S.; Mishra, Y.; Lamichhane, M. Out-Performing Bias-Corrected GCM Models and CMIP6-Based Precipitation and Temperature Projections for the Bagmati Irrigation Area. *Nepjol. Info* **2022**, *7*, 2022.
133. Cui, T.; Li, C.; Science, F.T.-E. Evaluation of Temperature and Precipitation Simulations in CMIP6 Models over the Tibetan Plateau. *Earth Space Sci.* **2021**, *8*, e2020EA001620. [CrossRef]
134. Song, S.; Zhang, X.; Yan, X. Evaluation of the Performance of CMIP6 Model Simulations for the Asian-Pacific Region: Perspectives from Multiple Dimensions. *Res. Sq.* **2022**. [CrossRef]
135. Lamichhane, M.; Mishra, Y.; Change, P.B.-J.E.S.C. Assessment of Future Water Availability and Irrigation Water Demand under Climate Change in the Kankai River Basin, Nepal. *J. Earth Sci. Clim. Change* **2022**, *13*, 2.
136. Wagesho, N.; Goel, N.; Journal, M.J.-H.S. Temporal and Spatial Variability of Annual and Seasonal Rainfall over Ethiopia. *Taylor Fr.* **2013**, *58*, 354–373. [CrossRef]
137. Zeleke, T.; Giorgi, F.; Mengistu Tsidu, G.; Diro, G.T. Spatial and Temporal Variability of Summer Rainfall over Ethiopia from Observations and a Regional Climate Model Experiment. *Theor. Appl. Climatol.* **2013**, *111*, 665–681. [CrossRef]

138. Teshome Ayana, M.; Wagesho, N.; Abdella Kemal Mohammed, I.; Kemal Mohammed, A. Assessment of the Impacts of Climate Change on Gibe-III Reservoir Using Reliability, Resilience and Vulnerability (RRV) Indices. *Int. J. Sci. Eng. Res.* **2017**, *8*, 1606–1628.
139. Demissie, T.A.; Saathoff, F.; Seleshi, Y.; Gebissa, A. Trends Of Hydro-Meteorological Data And Impact Of Climate Change On The Streamflow Of Gilgel Gibe 1 River Basin-Ethiopia. *Int. J. Curr. Res.* **2013**, *5*, 2988–2993.
140. Saathoff, F.W.; Barbaro, G.; Aldieri, L.; Tenfie, H.W.; Saathoff, F.; Hailu, D.; Gebissa, A. Selection of Representative General Circulation Models for Climate Change Study Using Advanced Envelope-Based and Past Performance Approach on Transboundary River Basin, a Case of Upper Blue Nile Basin, Ethiopia. *Sustainability* **2022**, *14*, 2140.
141. Choi, Y.W.; Campbell, D.J.; Eltahir, E.A.B. Near-Term Regional Climate Change in East Africa. *Clim. Dyn.* **2022**, *12*, 1–18. [CrossRef]
142. Camberlin, P. *Climate of Eastern Africa*; Oxford Research Encyclopedia of Climate Science: Oxford, UK, 2018.
143. Preethi, B.; Sabin, T.P.; Adedoyin, J.A.; Ashok, K. Impacts of the ENSO Modoki and Other Tropical Indo-Pacific Climate-Drivers on African Rainfall OPEN. *Nat. Publ. Gr.* **2015**, *5*, 16653.